

## **D6.2 – Report on the improved models of melting temperature and thermal conductivity for MOX fuels and JOG**

A. Magni (ENEA, Polimi), L. Luzzi (Polimi), P. Van Uffelen, D. Staicu (JRC),  
P. Console Camprini, P. Del Prete, A. Del Nevo (ENEA)

Version 2 – 08/10/2020

Document type	Deliverable
Document number	D6.2 version 2
Document title	Report on the improved models of melting temperature and thermal conductivity for MOX fuels and JOG
Authors	A. Magni (ENEA, Polimi), L. Luzzi (Polimi), P. Van Uffelen, D. Staicu (JRC), P. Console Camprini, P. Del Prete, A. Del Nevo (ENEA)
Release date	08/10/2020
Contributing partners	ENEA, JRC, POLIMI
Dissemination level	Public

Version	Short description	Main author	WP leader	Coordinator
2	Modification of correlations developed	A. Magni (Polimi) 07/10/2020	A. Del Nevo (ENEA) 08/10/2020	M. Bertolus (CEA) 08/10/2020

## SUMMARY

The current modelling of thermal properties (thermal conductivity, melting temperature) of mixed-oxide (MOX) nuclear fuels in Fuel Performance Codes (FPCs), e.g., GERMINAL, MACROS, TRANSURANUS, used in INSPYRE, is limited for various reasons. First, available experimental data concern mostly fresh MOX or Light Water Reactor (LWR) irradiation conditions, with only very few data about Fast Reactor (FR) MOX. Second, state-of-the-art correlations employed by FPCs mainly describe the temperature and porosity effects on the MOX thermal conductivity, without taking into account, e.g., the effect of the initial plutonium content. Task 6.3 of INSPYRE aims at overcoming these limitations by developing improved models for the thermal conductivity and the melting temperature of FR MOX, based on the most reliable and recent experimental data available in the open literature or accessible via the INSPYRE project. Additional experimental measurements performed in INSPYRE will also help to both further improve and validate the developed models herein presented.

This document is the update of the version 1 published in March 2020. Since then, further analyses and developments (justified in Section 2) were performed, leading to two main modifications:

- An exponential degradation of the thermal conductivity with burnup is considered instead of a linear dependency
- A few spurious experimental points were eliminated from the fitting process of the melting (solidus) temperature because they correspond to fuel compositions outside the range of application of the correlation developed (i.e., Pu content > 50 wt.%, O/M ~ 1.90).

This Deliverable first presents an exhaustive overview of the state of the art, both in terms of existing correlations (in literature and in FPCs) and available experimental data about MOX thermal conductivity and melting temperature. Then, the derivation and preliminary validation of new correlations oriented to FR MOX and dependent on all the significant parameters are described. Finally, the future model developments envisaged are outlined and the final assessment needed before the integration of these models in fuel performance codes is explained.

## CONTENT

SUMMARY.....	2
CONTENT.....	3
GLOSSARY .....	4
1 REVIEW OF THE STATE OF THE ART .....	5
1.1 State-of-the-art MOX thermal conductivity correlations .....	5
1.2 State-of-the-art MOX melting temperature correlations.....	8
1.3 Available experimental data.....	10
2 PROGRESS IN MODELLING THERMAL PROPERTIES FOR MOX FUELS IN FAST REACTOR CONDITIONS .....	13
2.1 Improved model for MOX fuel thermal conductivity.....	13
2.2 Improved model for MOX fuel melting temperature .....	22
3 JOINT OXYDE-GAINE (JOG): STATE OF THE ART AND ISSUES.....	28
4 CONCLUSION AND FUTURE DEVELOPMENTS.....	31
REFERENCES.....	32

## GLOSSARY

EBR	Experimental Breeder Reactor
EPMA	Electron Probe MicroAnalysis
ESFR-SMART	European Sodium Fast Reactor-Safety Measures Assessment and Research Tools
ESNII	European Sustainable Nuclear Industrial Initiative
EU	European Union
FBR	Fast Breeder Reactor
FCCI	Fuel-Cladding Chemical Interaction
FOC	Fuel Outer Compound
FP	Fission Product
FPC	Fuel Performance Code
FR	Fast Reactor
HM	Heavy Metal
HRP	Halden Reactor Project
IFPE	International Fuel Performance Experiments
INSPIRE	Investigations Supporting MOX Fuel Licensing for ESNII Prototype Reactors
JOG	Joint Oxyde-Gaine
JPNM	Joint Programme on Nuclear Materials
LWR	Light Water Reactor
MIMAS	MIcronized - MAStEr blend
MOX	Mixed-OXide
OCOM	Optimised CO-Milling
PIE	Post-Irradiation Examination
PWR	Pressurized Water Reactor
SBR	Short Binderless Route
TD	Theoretical Density

## 1 REVIEW OF THE STATE OF THE ART

### 1.1 State-of-the-art MOX thermal conductivity correlations

The thermal conductivity ( $k$ ) of a material, as a function of temperature ( $T$ ), is generally modelled as the sum of three temperature-dependent contributions

- the lattice vibration contribution, which is of the form  $1/(A+BT)$ ,
- the radiative contribution, proportional to  $T^3$ ,
- the electronic contribution, exponential in  $T$ .

In addition to these physically grounded temperature dependences, thermal conductivity correlations should also include other microstructure and irradiation effects. The inclusion of these effects leads to the effective thermal conductivity,  $k_{\text{eff}}$ , which typically takes into account the impact of fuel burnup (bu, in terms of dissolved fission products (FP), precipitated FPs or radiation damage), the deviation from fuel stoichiometry (usually in terms of oxygen-to-metal ratio, O/M), the fuel porosity and the plutonium content, as additional terms or as modifications of the temperature coefficients. These dependencies degrade the MOX thermal conductivity with respect to the thermal conductivity of fresh, stoichiometric, fully dense fuel. Further theoretical details about the thermal diffusivity and conductivity of various types of materials and nuclear fuels can be found in references [1]–[3].

Table 1 summarizes the existing correlations currently implemented in FPCs or published in the open literature. All the correlations listed in Table 1 have been obtained fitting out-of-pile thermal diffusivity measurements on LWR MOX [4]–[7], apart from the Wiesenack correlation [8], which derives from in-pile centreline temperature measurements on  $\text{UO}_2$  fuel rods at the Halden reactor and has subsequently been adapted to MOX fuel. Only one publication about thermal diffusivity measurements on FR MOX is available in literature [9]. Given the scarcity of available experimental data regarding hyper-stoichiometric  $\text{UO}_2$  or MOX fuel, the state-of-the-art correlations are all for stoichiometric or hypo-stoichiometric MOX fuel<sup>1</sup>. Most of the correlations refer to homogeneous MOX fuel, few of them are for heterogeneous MOX. They are all temperature-dependent, but many of them can only represent fresh MOX since they do not describe the burnup effect (degradation of the thermal conductivity).

A subset of eleven correlations, representative of the variety of existing correlations listed in Table 1, was selected to show the trend of the average effective thermal conductivity,  $k_{\text{eff}}$ . The selected correlations include the Philipponneau, the Carbajo, the Lanning-Beyer, the Wiesenack, the Van Uffelen-Schubert models implemented in the TRANSURANUS FPC [10]; two correlations for heterogeneous MOX [7], [11]; the Duriez-NFI model implemented in FRAPCON-3.5 [12]; the Duriez-Lucuta model taking into account the Lucuta correction factors for the burnup effects and recommended by Carbajo for high burnup MOX [13], [14]; a correlation for both homogeneous and heterogeneous MOX fuels obtained at JRC-ITU from thermal diffusivity measurements on industrially manufactured and commercially irradiated MOX fuel rods [4]. The selected correlations all include the fundamental influence of temperature and burnup on the effective thermal conductivity. The ranges considered are those of interest for MOX fuels ( $300 \text{ K} < T < 2500 \text{ K}$  and  $0 < \text{bu} < 200 \text{ GWd/tHM}$ ). Fixed values are assigned to the other parameters of the fuel thermal conductivity, i.e., stoichiometric fuel, 5 % atomic plutonium content and 95 % Theoretical Density (TD).

Figure 1 and Figure 2 show the average, for each  $(T, \text{bu})$  point, of the thermal conductivity values yielded by the selected correlations and the relative spread as a function of temperature and burnup.

<sup>1</sup>  $\text{UO}_2$  fuel becomes hyper-stoichiometric at high burnup, where few thermal conductivity data are available. On the other hand, the existence of hyper-stoichiometric  $\text{PuO}_{2+x}$  is not confirmed (only one controversial observation is available [74]). FR MOX fuel, whose chemical form is  $(\text{U}_{1-y}\text{Pu}_y)\text{O}_{2+x}$ , reaches hyper-stoichiometry at high burnup, where again no experimental data are available at present.

Thermal conductivity correlations: Effects considered												
	Year	Temperature	Burnup	Fresh fuel	Dissolved FP	Precipitated FP	Radiation damage generation	Radiation damage annealing	Oxygen-to-metal ratio (O/M)	Porosity	Pu content	References
Martin	1982	X		X								[15]
COMETHE	1982	X		X					X		X	[16]
Philipponneau	1992	X	X	X					X	X		[17], [18]
Baron-Hervé	1995	X		X					X		X	[16]
Wiesenack	1997	X	X	X						X		[8], [17]
Ohira-Itagaki	1997	X	X	X						X	X	[19]
Duriez-Lucuta	2000	X	X		X	X	X		X	X		[13], [20]
Lee (*)	2000	X	X	X					X	X	X	[11]
MATPRO	2001	X		X					X	X	X	[21]
Carbajo	2001	X	X		X	X	X		X	X		[14], [17]
Lanning, Beyer	2002	X	X	X	X			X	X	X		[12], [17]
Duriez-NFI	2005	X	X	X	X		X	X	X			[12], [20]
Kato	2011	X							X	X		[22]
Staicu	2011	X	X	X								[4]
Staicu (T <sub>irr</sub> )	2011	X	X	X								[4]
Amaya (*)	2011	X	X	X	X	X					X	[7]
Staicu-Barker (homogeneous MOX)	2013	X							X			[5]
Staicu-Barker model 1 (*)	2013	X		X					X		X	[5]
Staicu-Barker model 2 (*)	2013	X		X					X		X	[5]
Van Uffelen,-Schubert	2014	X	X	X						X		[17]
Van Uffelen-Schubert (conservative)	2014	X	X	X						X		[17]
ESNII+ Phenix	2017	X		X								[23]
ESNII+ Trabant	2017	X		X								[24]

Table 1: List of the state-of-the-art thermal conductivity correlations, available in literature or employed by FPCs, for MOX fuel. The (\*) symbol marks the correlations for heterogeneous MOX fuel.

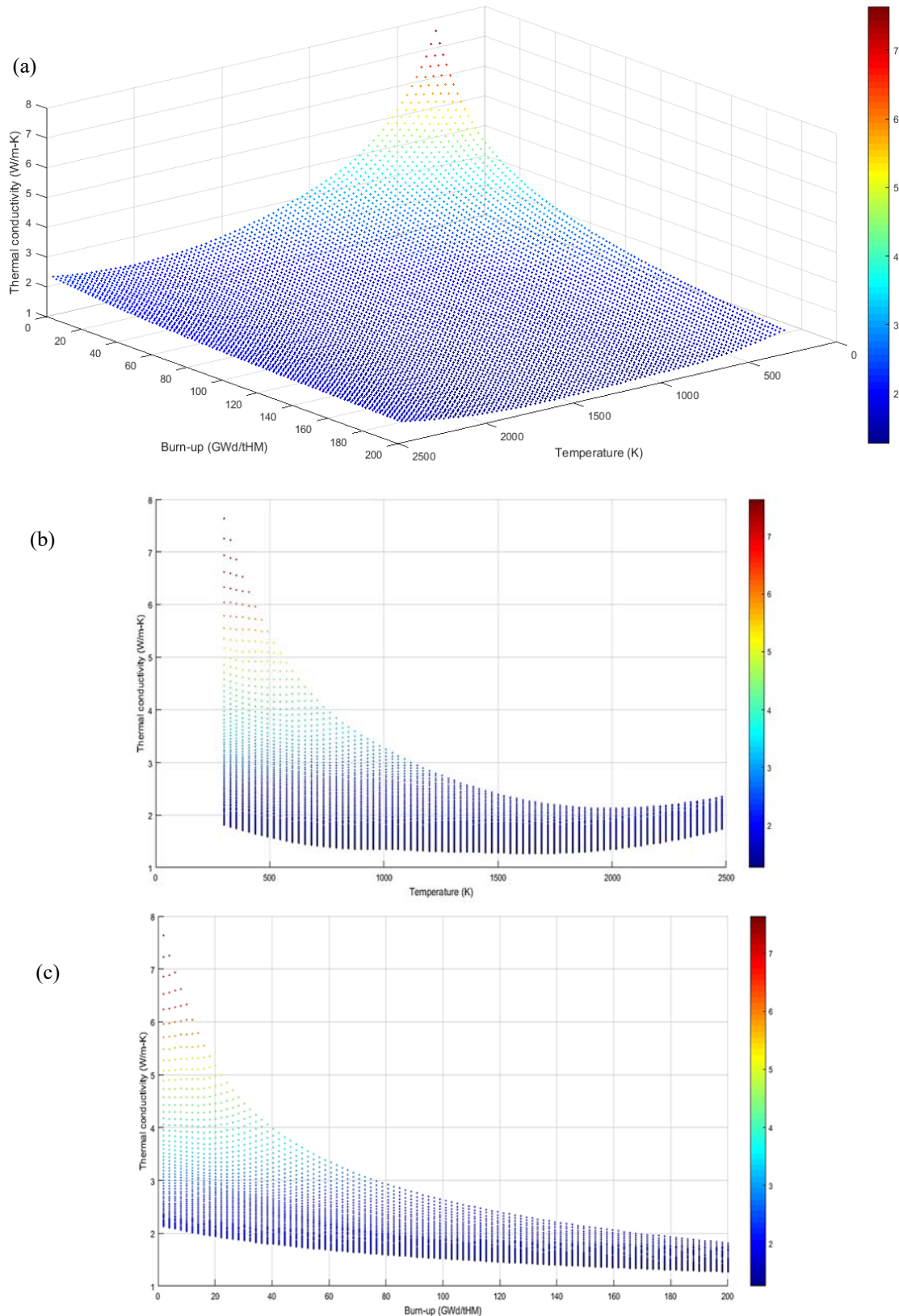


Figure 1: (a) 3D plot of the behaviour of the average effective thermal conductivity, yielded by the selected correlations for MOX fuel, as a function of fuel burnup and temperature. (b) 2D view of the dependence of the average thermal conductivity on the fuel temperature, from 300 to 2500 K, for all burnup values (represented by the vertical spread). (c) 2D view of the dependence of the average thermal conductivity on the fuel burnup, in the range (0, 200 GWd/tHM), for all temperature values (represented by the vertical spread).

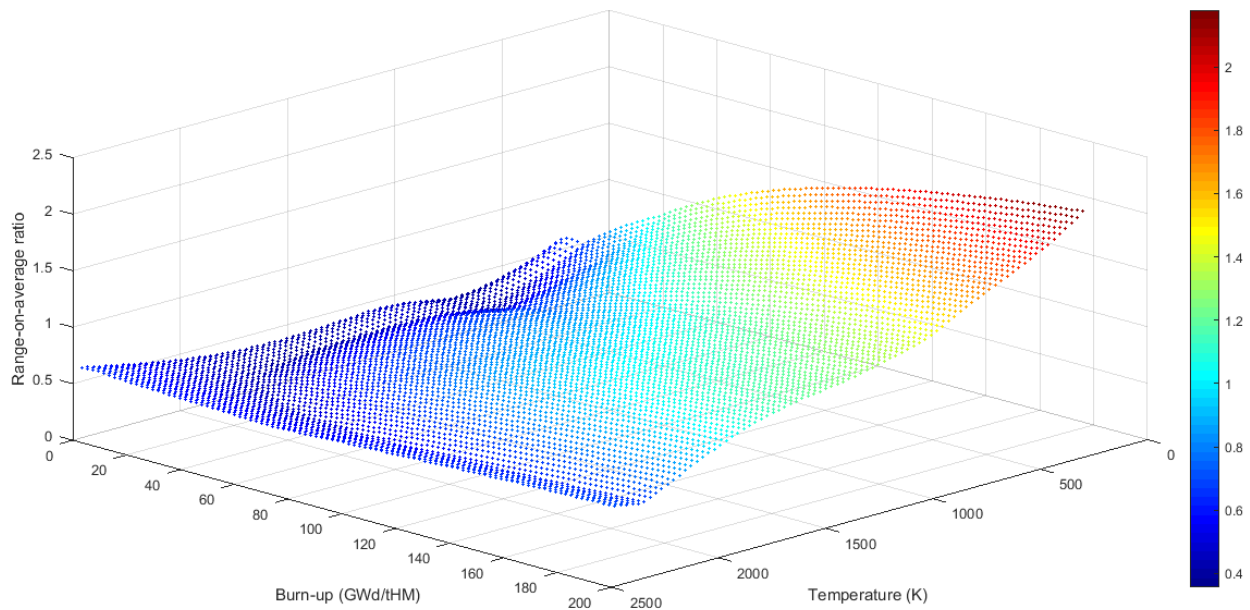


Figure 2: 3D plot of the relative spread of the thermal conductivity values, calculated as the ratio between the range spanned by the selected correlations and the average value at each grid point, as a function of fuel temperature and burnup.

It can be noticed from the 3D plot and the related 2D views of Figure 1 that the temperature behaviour of  $k_{\text{eff}}$  is mainly determined by the lattice contribution at low temperatures and by the electronic contribution at high temperatures, while  $k_{\text{eff}}$  is monotonically decreasing with increasing burnup. Figure 2 shows that the larger uncertainty on the thermal conductivity value is in the region of lower temperatures and higher burnup. The large spread at low temperature and high burnup could be mostly related to the lack of experimental data at such high burnup (up to 200 GWd/tHM). Indeed, those thermal conductivity values are calculated from state-of-the-art correlations extrapolated far outside from their burnup range of validation (limited to  $\sim 100$  GWd/tHM). Therefore, results are affected by the limited validity range of the correlations, causing a large spread out-of-range.

## 1.2 State-of-the-art MOX melting temperature correlations

The melting (or solidus) temperature ( $T_m$ ) of  $U_{1-y}Pu_yO_{2-x}$  MOX fuel is generally represented as a function of fuel burnup, stoichiometry (O/M) and plutonium content. The existing correlations for MOX fuel melting temperature, collected in Table 2, are built so that each aforementioned parameter causes a decrease of  $T_m$  with respect to that of pure  $UO_2$ . The degrading effects are evaluated on the basis of experimental observations on fuel specimens thermally arrested inside a tungsten or rhenium capsule [25]–[27]. These measurements show that the solidus temperature of MOX fuel decreases with increasing burnup, Pu content and deviation from stoichiometry. More recent measurements with laser heating techniques [28]–[30] yielded new results on the melting point of high-Pu enriched MOX fuels. It is recommended to use these recent results, together with those obtained in the framework of the ESNI+ Project [31].

Table 2 collects the state-of-the-art MOX solidus temperature correlations, detailing the effects included in each. The MATPRO and MAPLIB correlations are derived fitting experimental measurements on LWR MOX fuels, while the Tobbe, Pesl, Komatsu and Konno correlations are based on experimental data of MOX fuel for FR applications. The correlation by Konno [32] is the most complete and considered as the best state-of-the-art MOX melting temperature correlation.

	Year	Burnup	Pu content	Stoichiometry (O/M)	Am content	References
<b>Tobbe</b>	1975	X	X	X		[17]
<b>MAPLIB</b>	1977		X			[17]
<b>Adamson</b>	1985		X			[26]
<b>Pesl</b>	1987	X	X	X		[17]
<b>Komatsu</b>	1988	X	X	X		[27]
<b>European Catalogue</b>	1990	X	X	X		[31]
<b>MATPRO</b>	2001	X	X			[17], [21]
<b>Konno</b>	2002	X	X	X	X	[32]

Table 2: List of the state-of-the-art melting temperature correlations for MOX fuel available in literature or employed by FPCs.

The Tobbe, MAPLIB, Pesl and MATPRO correlations, which are implemented in the TRANSURANUS FPC [10], together with the Komatsu and Konno ones, were selected to evaluate an average predicted melting temperature, similarly to what was done for the thermal conductivity (Section 1.1). Figure 3 shows the average of the values yielded by these correlations as a function of fuel burnup and Pu content. A fixed value is assigned to the other parameters of the MOX fuel melting temperature, i.e., stoichiometric fuel ( $x = 0$ ). The relative uncertainty around the average values is shown in Figure 4.

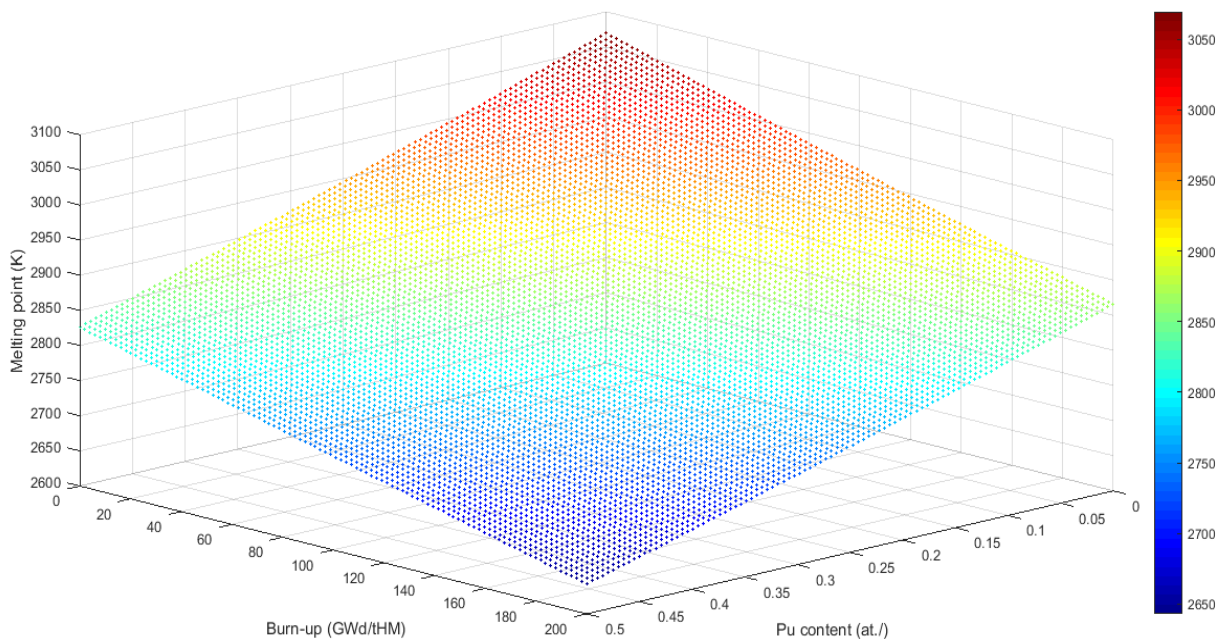


Figure 3: Behaviour of the average melting temperature of MOX fuel, yielded by the selected correlations, as a function of fuel burnup and plutonium content.

Figure 3 shows that the solidus temperature of MOX fuel, predicted by state-of-the-art correlations, decreases with both increasing fuel burnup and plutonium content. Furthermore, it can be seen from Figure 4 that the relative uncertainty on the average value significantly increases at high burnup, for all Pu contents.

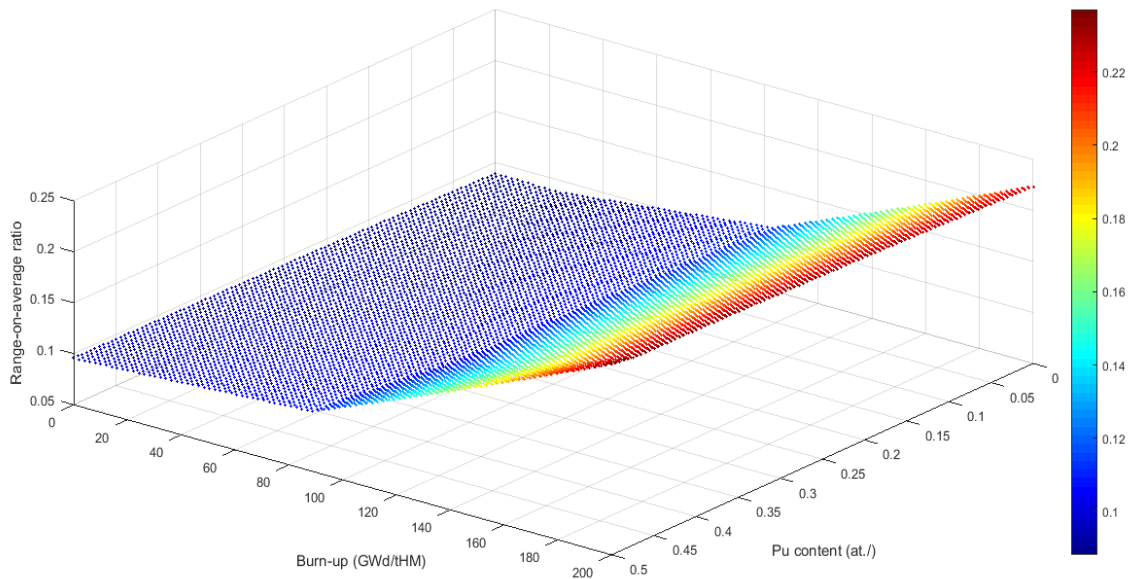


Figure 4: 3D plot of the relative uncertainty, calculated as the ratio between the range spanned by the selected melting point correlations and the average value in each grid point, as a function of fuel burnup and plutonium content.

This conclusion suggests to focus further investigations on high burnup conditions, where the solidus temperatures predicted by the current correlations are more scattered, i.e., more than 20 % spread on the average values predicted in the complete Pu content range considered (0 – 50 at.%).

### 1.3 Available experimental data

The available experimental data concerning melting temperature and thermal conductivity of MOX fuel were collected and analysed. The collected set includes measurements published in the open literature from the 60s, up to the recent ESNII+ reports (2017), describing measurements obtained on PHENIX and TRABANT fresh fuels and NESTOR-3 irradiated fuels. Some of these data have already been exploited for fitting by previous works proposing empirical correlations for  $k$  and  $T_m$ , reported in Sections 1.1 and 1.2 of this document. The MOX thermal conductivity experimentally proves to decrease with increasing temperature (down to a minimum value at around 1500-2000 K, after which it slightly increases), burnup, Pu content, deviation from stoichiometry (in the hypo-stoichiometric range) and porosity. MOX melting temperature experimentally decreases, with respect to  $UO_2$  melting temperature, with increasing burnup, Pu content and deviation from stoichiometry. In Table 3 and Table 4, literature works providing experimental measurements of MOX thermal conductivity and melting temperature are listed, together with the description of the kind of measured fuel and measurement technique employed.

As described in Sections 1.1 and 1.2, existing MOX thermal conductivity and melting temperature correlations generally neglect some fundamental parameters, particularly the plutonium content and the fuel burnup effect. Thanks to a complete set of available experimental data, new and improved (i.e., more comprehensive and accurate with respect to the available data considered) correlations describing the degradation of MOX thermal conductivity and melting temperature due to all the aforementioned effects can be built.

Reference	Measured fuel	Experimental technique
<b>Gibby, 1971</b> [33]	Fresh (U,Pu)O <sub>2</sub> , coprecipitated solid solutions containing 5, 12, 20, 25, 30 wt.% PuO <sub>2</sub> , measured at T from 100 to 1200 °C	Laser heat pulse for thermal diffusivity, thermal conductivity obtained from specific heat capacity and density
<b>Yamamoto <i>et al.</i>, 1993</b> [9]	Irradiated (U,Pu)O <sub>1.97</sub> up to 35 GWd/tHM at LHR from 12 to 38 kW/m, with fresh fuel density 93-94 % TD and Pu content ~ 18 and 28 wt.%	Laser-flash method for thermal diffusivity, thermal conductivity obtained from specific heat capacity and density
<b>Duriez <i>et al.</i>, 2000</b> [34]	Fresh PWR MOX with Pu contents from 3 to 15 wt.% and O/M ratio from 1.95 to 2.00, measured at T from 700 to 2300 K	Laser-flash method for thermal diffusivity, thermal conductivity obtained from specific heat capacity (Kopp's law) and density
<b>Inoue, 2000</b> [35]	Reports exp. data from Hetzler 1967, Van Craeynest 1968, Laskiewicz 1971, Fukushima 1983, Elbel 1985 & 1988, Bonnerot 1988 (fresh fast reactor MOX, 100 % TD, Pu content from 20 to 30 wt.%, O/M from 1.96 to 2.00	Thermal diffusivity measured by radial heat flux (Hetzler, Laskiewicz), laser-flash (Fukushima, Van Craeynest, Bonnerot), and electron beam (Elbel) techniques
<b>Carbajo <i>et al.</i>, 2001</b> [14]	Reports high T exp. data from Weilbacher 1968 & 1972, Van Craeynest 1968, Schmidt 1971, Bonnerot 1988, Ronchi 1998, laboratory MIMAS MOX (fresh MOX, 95 % TD, Pu content from 3 to 20 %, O/M from 1.93 to 2.00)	Laser-flash method for thermal diffusivity and drop calorimetry technique for specific heat capacity
<b>Cozzo <i>et al.</i>, 2010</b> [36]	Irradiated homogeneous laboratory SBR MOX, up to bu of 35 GWd/tHM, with fresh fuel Pu content of 3.7 wt.%, 95 % TD, O/M 2.00, measured at T from 520 to 1460 K (reports also data from Lanning 2004 on similar MOX)	Shielded laser-flash device for thermal diffusivity; specific heat capacity assumed equal to fresh fuel value
<b>Staicu <i>et al.</i>, 2011</b> [4]	Irradiated (44 GWd/tHM) OCOM, MIMAS and SBR MOX, homogeneous and heterogeneous, 95 % TD, with fresh fuel Pu content from 3.5 to 6.9 wt.%, measured at T from 500 to 1500 K	Shielded laser-flash device for thermal diffusivity; specific heat capacity assumed equal to fresh fuel value
<b>Staicu, Barker, 2013</b> [5]	Fresh SBR, sol-gel and MIMAS heterogeneous LWR MOX, 94.5 – 96 % TD, Pu content from 4.8 to 11.1 wt.%, O/M approx. 2.00, measured at T from 500 to 1550 K	Shielded laser-flash device for thermal diffusivity; specific heat capacity assumed equal to fresh fuel value
<b>ESNII+ D7.34, 2017</b> [24]	Fresh TRABANT MOX fuel: density from ~93 to 95% TD, Pu content of 40 and 45 mol%, O/M from 1.96 to 2.00, measured at T between 500 and 1600 K	Immersion technique for the density, Differential Scanning Calorimetry for the specific heat capacity, laser-flash method for the thermal diffusivity
<b>ESNII+ D7.41, 2017</b> [23]	Fresh PHENIX MOX fuel: 95 % TD, Pu content 24 mol%, O/M 2.00, measured at T between 500 and 1600 K	Differential Scanning Calorimetry for the specific heat capacity, laser-flash method for the thermal diffusivity
<b>ESNII+ D7.42, 2017</b> [37]	Irradiated NESTOR-3 MOX fuel: 96 % TD, Pu content 24 mol%, O/M = 2.00, measured at T between 500 and 1600 K	Laser-flash method for the simultaneous measurement of thermal diffusivity and specific heat capacity (with a calorimeter in the sample position)

Table 3: List of references for MOX thermal conductivity experimental data, with details about the fuel material and the experimental technique employed.

Reference	Measured fuel	Experimental technique
<b>Lyon, Baily, 1967</b> [25]	Fresh MOX, O/M = 2.00, Pu content up to 85 mol%	Sample heating in a W capsule
<b>Adamson et al., 1985</b> [26]	Reports data from Reavis 1972 (fresh and irradiated MOX at 43 and 76 GWd/tHM, O/M = 1.97 and 1.98, 25 mol% Pu content) and from Aitken, Evans 1968 (fresh MOX, O/M = 2.00, Pu content from 20 to 60 mol%)	Sample heating in a W capsule (Aitken, Evans 1968), Differential Thermal Analysis method (Reavis 1972)
<b>Tachibana et al., 1985</b> [38]	Irradiated MOX with burnup between 8.2 and 43 GWd/tHM, O/M = 1.99, Pu content = 17.7 mol%, Am content = 0.13 mol%	Thermal arrest technique on sample in a W capsule
<b>Komatsu et al., 1988</b> [27]	Irradiated MOX with burnup between 8 and 112 GWd/tHM, O/M = 2.00, Pu content of ~ 20 and 23 mol%. Reports also data on irradiated MOX from Krankota and Craig, 1969	Sample heating in a W capsule, pyrometer measurements
<b>Yamamoto et al., 1993</b> [9]	Irradiated MOX with burnup between 4 and 124 GWd/tHM, O/M between 1.93 and 1.98, Pu content from ~ 28 to 33 mol%	Thermal arrest technique on sample in a W capsule
<b>Konno, Hirosawa, 1998</b> [39]	Fresh and irradiated MOX, burnup from 0 to 124 GWd/tHM, O/M between 1.95 and 1.98, Pu content of ~ 30 mol%, Am content between 0.04 and 0.9 mol%	Thermal arrest technique on sample in a W capsule
<b>Konno, Hirosawa, 2002</b> [32]	Irradiated MOX with burnup between 8.2 and 110.9 GWd/tHM, O/M = 1.98, Pu content = 17.5 mol%, Am content = 0.13 mol%	Thermal arrest technique on sample in a W capsule
<b>Kato et al., 2008 (a)</b> [40]	Fresh MOX, O/M from 1.922 to 2.000, Pu content from 11.7 to 60.0 mol%, Am content from 0.3 to 3.3 mol%	Sample heating in a Re or W capsule, analysis of pyrometer thermograms
<b>Kato et al., 2008 (b)</b> [41]	Fresh MOX, O/M from 1.942 to 2.000, Pu content between 12 and 40 mol%	Sample heating in a W capsule, analysis of pyrometer thermograms
<b>Hirosawa et al., 2011</b> [42]	Fresh and irradiated FR MOX with burnup from 0 to 112.5 GWd/tHM, O/M from 1.96 to 1.99, Pu content between 31 and 35 mol%	Sample heating in an inner Re capsule + outer W capsule, Thermal arrest technique
<b>De Bruycker et al., 2011</b> [28]	Fresh MOX, O/M = 2.00, Pu content from 75 to 90 mol%	Laser heating and analysis of pyrometer thermograms or Reflected Light Signal method
<b>Bohler et al., 2014</b> [29]	Fresh MOX, O/M = 2.00, Pu content from 3.7 to 90 mol%	Laser heating and analysis of pyrometer thermograms
<b>Prieur et al., 2015</b> [43]	Fresh MOX, O/M = 1.98, Pu content = 22 mol%, Am content = 3.5 mol%	Laser heating and analysis of pyrometer thermograms
<b>Strach et al., 2016</b> [30]	Fresh MOX, O/M = 2.00, Pu content from 14 to 54 wt%	Thermal arrest technique on samples obtained from UO <sub>2</sub> and PuO <sub>2</sub> powders. Measurements in Ar atmosphere
<b>ESNII+ D7.41, 2017</b> [23]	Fresh PHENIX MOX, 95% TD, Pu content 24 mol%, O/M = 2.00 (stoichiometric) and 1.978 (hypo)	Laser heating and fast multi-channel pyrometry

Table 4: List of references for MOX melting temperature experimental data, with details about the fuel material and the experimental technique employed.

All the thermal conductivity and melting temperature experimental data come from hypo-stoichiometric or stoichiometric MOX fuel, for a total of about one thousand measurements of thermal conductivity and 170 points of melting temperature. The experimental uncertainty, principally related to the measurement method, is between 10 and 20 % of the measured value for the thermal conductivity, while an uncertainty between 10 and 70 K is reported on the melting temperature data.

Among all the available data, a subset of the “best” ones can be selected, considering for example the experimental technique used for the measurements. In particular, the melting temperature measurements on samples heated in a W capsule, a technique employed in older works, should be excluded as it has been proved that tungsten at high temperatures can contaminate the fuel sample, causing a significant lowering of its melting point [28], [40], [42]. Instead, the recent measurements, including those achieved in the framework of the ESNII+ Project using up-to-date experimental facilities and procedures [23], [24], [37], are herein considered as reference for both thermal conductivity and melting temperature.

It is important to note that the MOX fuel characteristics of plutonium content, stoichiometry (O/M ratio) and porosity, which influence significantly both the material thermal conductivity and melting point, are reported in the experimental works considered mostly as those measured on fresh fuel. Although fuel burnup has a strong impact on the fuel microstructure, only Konno and Hirosawa [32], [39] report the modified value of plutonium content and stoichiometry after the irradiation of the sample up to a certain burnup.

The selection of the best experimental data among the available ones (Table 3 and Table 4) is a fundamental step towards the derivation of novel complete correlations describing FR MOX thermal conductivity and melting temperature.

## 2 PROGRESS IN MODELLING THERMAL PROPERTIES FOR MOX FUELS IN FAST REACTOR CONDITIONS

### 2.1 Improved model for MOX fuel thermal conductivity

The first step towards the proposal of an original MOX thermal conductivity correlation is the selection of a suitable set of experimental data among all the measurements available in literature (Table 3). Focusing on the most recent data, considered as the most reliable, for fresh MOX fuel, thermal conductivity data by Staicu *et al.*, 2013 [5] concerning both homogeneous and heterogeneous MOX fuels, as well as data on PHENIX and TRABANT MOX samples obtained in the frame of the ESNII+ Project (2017) [23], [24], are selected. Given the lack of recent high-temperature data, older high-temperature data from Ronchi *et al.*, 1998 and Bonnerot *et al.*, 1988 [14], still considered as a reference in the field, are included in the fitting dataset. For irradiated MOX fuel, the ESNII+ Project measurements on high burnup NESTOR-3 MOX fuel ([37], 84 and 130 GWd/tHM) were selected, together with data by Yamamoto *et al.*, 1993 [11], to derive an accurate correlation also at low and moderate burnups (samples at 8, 19 and 35 GWd/tHM). It is worth noting that these are the only data currently available in the open literature on thermal conductivity of irradiated fast reactor MOX fuel. Details about the MOX thermal conductivity data selected are given in Table 5.

Fresh MOX fuel		
Reference	Measured fuel	Experimental technique
<b>Bonnerot <i>et al.</i>, 1988 (reported by Carbajo <i>et al.</i>, 2001) [14]</b>	Fresh MOX, 95% TD, [Pu] = 20 wt.%, O/M 1.98, measured at $T$ between 1500 and 2260 K	Laser-flash method for thermal diffusivity and drop calorimetry technique for specific heat capacity
<b>Ronchi <i>et al.</i>, 1998 (reported by Carbajo <i>et al.</i>, 2001) [14]</b>	Fresh MOX, 95% TD, [Pu] = 5 wt.%, O/M 2.00, measured at $T$ between 2050 and 2700 K	Laser-flash method for thermal diffusivity and drop calorimetry technique for specific heat capacity
<b>Staicu <i>et al.</i>, 2013 [5]</b>	Fresh SBR, sol-gel and MIMAS heterogeneous LWR MOX, 94.5-96% TD, [Pu] = 4.8 to 11.1 wt.%, O/M approx. 2.00, measured at $T$ from 500 to 1550 K	Shielded laser-flash device for thermal diffusivity; specific heat capacity assumed equal to fresh fuel value
<b>ESNII+ D7.34, 2017 [24]</b>	Fresh TRABANT MOX fuel: density from ~93 to 95% TD, [Pu] 40 and 45 mol.%, O/M from 1.96 to 2.00, measured at $T$ between 500 and 1600 K	Immersion technique for the density, Differential Scanning Calorimetry for the specific heat capacity, laser-flash method for the thermal diffusivity
<b>ESNII+ D7.41, 2017 [23]</b>	Fresh PHENIX MOX fuel: 95% TD, [Pu] = 24 mol.%, O/M 2.00, measured at $T$ between 500 and 1600 K	Differential Scanning Calorimetry for the specific heat capacity, laser-flash method for the thermal diffusivity
Irradiated MOX fuel		
Reference	Measured fuel	Experimental technique
<b>Yamamoto <i>et al.</i>, 1993 [9]</b>	Irradiated (U,Pu) <sub>0.97</sub> (8, 19, and 35 GWd/tHM) at LHR from 12 to 38 kW/m, with fresh fuel density 93-94% TD, [Pu] = ~18 wt.%	Laser-flash method for thermal diffusivity, thermal conductivity obtained from specific heat capacity and density
<b>ESNII+ D7.42, 2017 [37]</b>	Irradiated NESTOR-3 MOX fuel (84 and 130 GWd/tHM), 96% TD, [Pu] = 24 mol.%, O/M = 2.00, measured at $T$ between 500 and 1600 K	Laser-flash method for the simultaneous measurement of thermal diffusivity and specific heat capacity (with a calorimeter in the sample position)

Table 5: List of selected experimental data of fresh and irradiated MOX thermal conductivity, with details about the fuel material and the experimental technique employed.

The model development is performed in two steps. First, a correlation for fresh MOX thermal conductivity is derived based on the selected fresh MOX experimental data. Then, a correlation describing the thermal conductivity evolution during irradiation is obtained by including the fresh MOX conductivity in a burnup dependent formulation, fitted on the selected data from irradiated fuel. Both fresh and irradiated MOX data used to derive the new conductivity correlation are collected in Table 5.

In the first step, the thermal conductivity correlation to be fitted to the selected experimental data is defined, having a physically grounded expression  $k_0(T, x, [Pu], p)$ , depending on the three temperature contributions (lattice vibration (phononic), radiative and electronic), corrected with the inclusion of plutonium and stoichiometry-dependent terms in the lattice contribution, and of a porosity corrective factor. Specifically, the stoichiometry and plutonium content effects are introduced in the model as modifications to the  $A$  and  $B$  coefficients of the lattice vibration term. Hence, the functional form of the thermal conductivity correlation for fresh MOX,  $k_0$ , chosen as starting point of the fitting procedure, is

$$k_0(T, x, [Pu], p) = \left( \frac{1}{A + BT} + CT^3 + \frac{D}{T^2} e^{-\frac{E}{T}} \right) (1 - p)^{2.5} \quad (1)$$

$$\text{with } A = A_0 + A_x \cdot x + A_{Pu}[Pu] \text{ and } B = B_0 + B_x x + B_{Pu}[Pu],$$

Where,  $x$  is the deviation from stoichiometry ( $x = 2 - O/M$ ),  $[Pu]$  is the MOX plutonium content and  $(1 - p)^{2.5}$  is the modified Loeb porosity corrective factor, adopted, e.g., in the Van Uffelen-Schubert correlation implemented in the TRANSURANUS FPC [10].  $A_0, A_x, A_{Pu}, B_0, B_x, B_{Pu}, C, D, E$  are the correlation coefficients to be fitted on the selected set of fresh MOX experimental data.

The linear dependency on the deviation from stoichiometry differs from the square root term proposed by a few existing correlations for MOX fuel [35], [44], for  $UO_2$  [45], [46] and emerging from Molecular Dynamics calculation results (e.g., [47]), but is supported by the majority of state-of-the-art models available in literature and in fuel performance codes [12], [14], [15], [34], [48]. Furthermore, we included the plutonium effect, in contrast with previous works that excluded it in the ranges 3–15 [34] and 15–30 [44] wt.%  $PuO_2$ . This inclusion finds confirmation in experimental and modelling results on MOX [5], [48], as well as in theoretical works about thermal diffusivity and conductivity of various types of materials and nuclear fuels [1]–[3].

The statistical significance and weight of each term of the correlation, with respect to the chosen fitting dataset, is evaluated with a statistical analysis. A multi-dimensional fit has been performed using both MATLAB tools [49] and the R code [50], an open source software with built-in statistical analysis capabilities, to obtain, in addition to the regressor values, the related p-values, the confidence intervals and the fit residuals. The significance of each term of the starting correlation was evaluated taking the p-value associated to each regressor as figure of merit (compared to a threshold p-value of 5 %, corresponding to a 95 % confidence on the significance of a regressor). In this way, performing a hypothesis test through the R statistical code tools, a regressor is kept in the final form of the correlation if the associated p-value is below 5 %, otherwise it is rejected as statistically insignificant, i.e., not well represented by the fitting dataset. It is worth highlighting that the p-values obtained from the hypothesis test, like the other results of the fitting procedure, strongly depend on the dataset on which the fit is performed.

A non-linear fit is an iterative procedure searching for convergence on the regressor values and therefore requires initial values for the fit coefficients. The regressor initial values are fixed to the values employed by existing correlations for the same kind of terms [17]–[19]. The stability and independence of the resulting fit coefficients on the initial values was tested within reasonable ranges of the initial values themselves. These tests proved that the coefficients hold true performing further iterations and that the non-linear fitting procedure is slightly affected by their initial values.

The statistical significance of the regressor was tested against the entire set of selected experimental data (Table 5), as well as against sub-sets composed by data that, among the selected ones, depend on only one among the  $(T, x, [Pu])$  variables. Moreover, the discrimination between low and high temperature data was tested, fitting only the lattice vibration term on the low-T data and the radiative and electronic terms on the high-T data. The aim of these partial fits is to achieve higher confidence on the significance of each correlation regressor, focusing only on the p-values. The fit of  $k_0$  over all the selected fresh MOX data shows p-values lower than 5% for the fit coefficients  $A_0, B_0, B_{Pu}, D, E$  ( $<10^{-8}, <10^{-16}, 1.5\%, 4\%, <10^{-14}$ , respectively), and significantly higher than 5% for the fit coefficients  $A_x, A_{Pu}, B_x, C$  (39%, 10%, 46%, 25%<sup>2</sup>, respectively, values depending on the experimental ranges covered by the data composing the fitting dataset). Additionally, the results of the partial fits confirmed the exclusion of the regressors  $B_x$  and  $C^2$ , since they are featured by p-values much higher than 5% both on the entire set and on the sub-sets (i.e., on the sub-sets of data corresponding to low temperature and constant p and [Pu], and to high temperature, respectively). As for the regressor  $A_x$ , although its p-value is higher than 5% on both the entire set (39%) and the sub-set of low T, constant [Pu] and p data (14%), it is closer to

<sup>2</sup> The radiative contribution to the thermal conductivity,  $CT^3$ , dominates at very high temperatures, a region where the available MOX thermal conductivity experimental data are scarce. Instead, the exclusion of the regressor  $B_x$  is physically justified by the fact that B describes the phonon-phonon collisions, while A depends on impurities or alloying additions, so it is apt to include the fuel stoichiometry effect.

the 5 % threshold than the  $B_x$  p-value on the same sub-set (75%).  $A_x$  is therefore kept in the  $k_0$  correlation, in order to have the stoichiometry effect represented in the lattice contribution. The regressor  $A_{Pu}$  is also preserved in the correlation, since well represented by the sub-set of T and [Pu]-dependent data (p-value lower than 5%).

The form of the correlation for fresh MOX thermal conductivity obtained from the statistical assessment is

$$k_0(T, x, [Pu], p) = \left( \frac{1}{A_0 + A_x \cdot x + A_{Pu} \cdot [Pu] + (B_0 + B_{Pu}[Pu])T} + \frac{D}{T^2} e^{-\frac{E}{T}} \right) (1 - p)^{2.5} \quad (2)$$

The fit of this statistically assessed  $k_0$  functional form on the complete set of selected fresh MOX data leads to the results collected in Table 6. The final regressor values were obtained imposing their positivity as a constraint in order to guarantee their physical sense. In this way all the effects included degrade the thermal conductivity, as expected from experimental observations shown in Table 3, as well as in other literature works, e.g., [4], [36], [48], and theoretical considerations about phonon interactions with lattice defects. The regressor values reported in Table 6 are valid for temperature expressed in K, plutonium concentration [Pu] in atomic fraction and porosity p in TD fraction. The fresh MOX thermal conductivity,  $k_0$ , is calculated in W/(m·K).

Regressor	Units	Estimate
$A_0$	m·K/W	0.01926
$A_x$	m·K/W	$1.06 \cdot 10^{-6}$
$A_{Pu}$	m·K/W	$2.63 \cdot 10^{-8}$
$B_0$	m/W	$2.39 \cdot 10^{-4}$
$B_{Pu}$	m/W	$1.37 \cdot 10^{-13}$
$D$	W·K/m	$5.27 \cdot 10^{+9}$
$E$	K	17109.5

Table 6: Results of the fit of the statistically assessed  $k_0(T, x, [Pu], p)$  correlation (Eq. 2) on the whole set of the selected fresh MOX thermal conductivity data.

It was verified that the fit coefficient values in Table 6 are kept stable performing other fitting iterations. The effect of plutonium content and deviation from stoichiometry (in the hypo-stoichiometric range) on the MOX thermal conductivity obtained is minor if compared to the temperature effect, as shown by the coefficient values reported in Table 6. The values of  $A_x$ ,  $A_{Pu}$  and  $B_{Pu}$  are orders of magnitude lower than  $A_0$  and  $B_0$ , which are the basic coefficients composing a lattice vibration contribution to thermal conductivity only dependent on temperature. A slight effect of the plutonium content in the range between 0 and 45 wt.% is supported by literature works concerning both LWR [34] and FBR MOX [44], as well as by the recent measurements on TRABANT fresh MOX fuel performed in the framework of the ESNI+ H2020 Project [24]. On the contrary, the effect of deviation from stoichiometry reveals itself negligible due to the lack of data points for significantly hypostoichiometric conditions. Most of the fresh MOX data are obtained on samples with O/M = 2.00 [22], [23]. Additional experimental data are necessary to assess further the impact of hypostoichiometry on the MOX thermal conductivity.

The comparison between the thermal conductivity data, on which the  $k_0(T, x, [Pu], p)$  correlation (Eq. 2) has been built, and the fit estimations as a function of temperature, is shown in Figure 5. It is worth noting that the agreement between data and estimations is remarkable, both at low and high temperatures. The average residual is about  $2 \cdot 10^{-1}$  W/(m·K), similar to the experimental uncertainty, which for these data is between 10 and 20 % of the measured value [5], [9], [14], [23], [24], [37]. The fit

residuals in  $T, x, [Pu]$ , not shown here for the sake of brevity, are all randomly distributed, with no clear trends. This shows that it is not necessary to correct the fresh MOX thermal conductivity correlation obtained with mixed effects terms (present in some existing thermal conductivity correlations [7], [11], [20], [21]) or additional higher order terms. Such improvements would only be justified in the case of fit residuals following a clear trend as a function of one of the correlation variables. Data assimilation techniques such as Bayesian calibration methods (e.g., [51]) could be considered in the future to perform potential model adjustments when more experimental data become available.

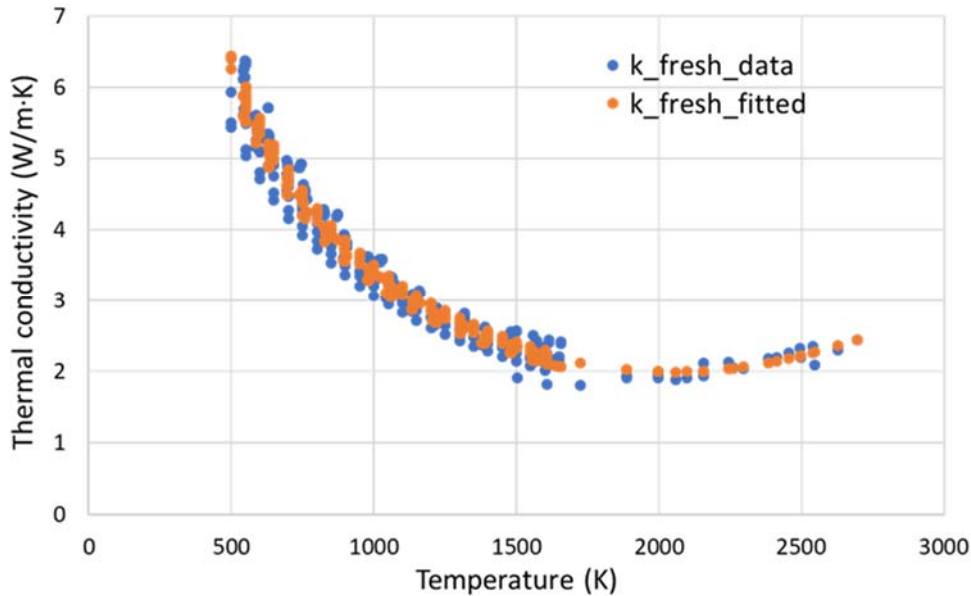


Figure 5: Temperature dependence of the fresh MOX thermal conductivity experimental data (blue dots, Table 5), considered as fit dataset, compared to the corresponding predictions provided by the correlation fitted on these data (orange dots).

Another parameter impacting significantly the thermal conductivity is the burnup. We chose an exponential degradation of the thermal conductivity of irradiated MOX fuel with fuel burnup ( $k_{irr}$ , Eq. 3). This is derived from the vast amount of data available in the HRP [52] and IFPE [53] databases for LWR fuels at extended burnup values, pointing out to a thermal conductivity degradation [54]. This is attributed to the accumulation of point defects and fission products, which increase the phonon scattering (represented by the A term in the lattice thermal conductivity model). The thermal conductivity degradation, however, was indicated to saturate beyond approximately 50 GWd/tHM in the mid-1990s [55]. The correlation hence reads

$$k_{irr}(T, x, [Pu], p, bu) = k_{inf} + (k_0(T, x, [Pu], p) - k_{inf}) \cdot e^{-\frac{bu}{\varphi}} \quad (3)$$

Where,  $k_0(T, x, [Pu], p)$  is the thermal conductivity of fresh MOX calculated using Eq. 2 (employing the coefficient values collected in Table 6),  $bu$  is the fuel burnup in GWd/tHM,  $k_{inf}$  is the asymptotic thermal conductivity at high burnup based on the only two available sets of experimental data on irradiated FR MOX ([9], [37], see Table 5),  $\varphi$  is a coefficient fitted again on [9], [37].

This formulation is applicable to fresh MOX fuel, since at zero burnup  $k_{irr}(T, x, [Pu], p, bu) = k_0(T, x, [Pu], p)$ , from Eq. 3. The asymptotic lower limit for the thermal conductivity degradation with burnup ( $k_{inf}$ ), in principle depending on plutonium content, deviation from stoichiometry and porosity of the fuel of interest, was chosen based on the available experimental data. Its value is derived from an extrapolation of the experimental behaviour of thermal conductivity from Yamamoto and NESTOR-3

data at the highest common temperature of measurement (i.e., 1480 K, corresponding to the lowest thermal conductivity data) to a burnup of 200 GWd/tHM, considered as the limit fuel burnup for Generation IV reactor applications [56], [57]. The correlation coefficients are collected in Table 7, including the value of  $\varphi$  resulting from data fitting.

Regressor	Units	Estimate
$K_{inf}$	W/(m·K)	1.755
$\varphi$	GWd/tHM	128.75

Table 7: Values of the coefficients of the  $k_{irr}(T, x, [Pu], p, bu)$  correlation (Eq. 3), fitted on the set of irradiated MOX thermal conductivity data [9], [37].

The agreement between the values calculated by the new correlation (Eq. 3) and the irradiated MOX thermal conductivity data from NESTOR-3 [37] and Yamamoto's samples [9] is satisfactory. The comparison between predicted values and Yamamoto's experimental measurements is shown in Figure 6 (NESTOR-3 data are not shown since they are confidential). The overall average residual is approximately 10 %, compared to an experimental uncertainty equal to  $\sim 8\%$  and  $\sim 30\%$  for NESTOR-3 and Yamamoto's datasets, respectively.

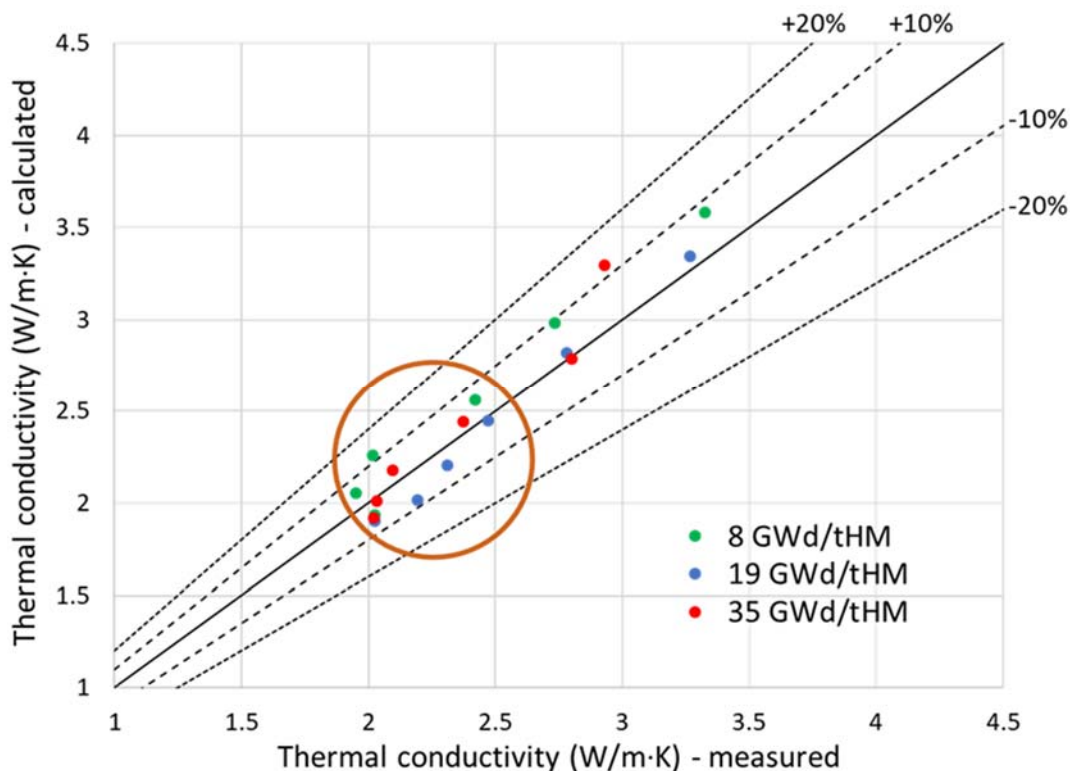


Figure 6: Comparison between the irradiated MOX thermal conductivity data by Yamamoto [9] and the corresponding predictions given by the new correlation developed for irradiated MOX (Eq. 3). The points circled in orange correspond to the range of thermal conductivity values foreseen during the operation of Generation IV reactors, for which the correlation predictions are the most accurate.

It can be seen in Figure 6 that the thermal conductivity values predicted by the new correlation all lie inside a 20% error band with respect to Yamamoto's experimental measurements. Moreover, the agreement is even better (10 % maximum deviation) in the range of thermal conductivity values between 2 and 2.5 W/(m·K) (points circled in Figure 6), corresponding to the target temperature and

burnup operative conditions foreseen for Generation-IV fast reactors, i.e., peak fuel temperature in excess of  $\sim 2300$  K and discharge fuel burnup of 150 - 200 GWd/tHM [56], [57].

The ranges of applicability of the newly developed correlations for MOX fuel thermal conductivity, corresponding to the ranges covered by the considered experimental data, are:

- Temperature, T: [500, 2700] K
- Deviation from stoichiometry, x: [0, 0.07] (hypo-stoichiometry)
- Plutonium content, [Pu]: [0, 45] wt.%
- Porosity, p: [0, 7] %TD
- Burnup, bu: [0, 130] GWd/tHM.

The main limitation of the correlation developed is therefore the range of discharge burnup, which may exceed 130 GWd/tHM in Generation IV fuel types. Data assimilation techniques could be envisaged for a progressive upgrade of the correlation as soon as more experimental results on representative irradiated FBR MOX fuels become available.

In Figure 7, the behaviour of the new MOX thermal conductivity correlation as a function of fuel temperature is compared with two main state-of-the-art correlations, by Philipponneau [18] and Van Uffelen-Schubert [10], developed for LWR MOX. Results refer to stoichiometric MOX, i.e.,  $x = 0$ , with 20 at.% initial Pu content and 5% porosity at 10 GWd/tHM burnup. The new correlation (blue dots) predicts the highest value at low temperature and a thermal conductivity value between 2 and 2.5 W/(m·K) at 2500 K, similarly to the other correlations considered. Table 8 reports the root mean square errors of the three correlations considered compared to the entire set of available thermal conductivity experimental data (concerning both fresh and irradiated MOX, Table 5). The error of the correlation developed in this work is less than half the error of the two state-of-the-art correlations considered for comparison [10], [44].

Figure 8 shows the capability of the new correlation (blue dots) to reproduce the thermal conductivity behaviour of  $UO_2$  fuel as a function of temperature. It is compared (setting zero Pu initial content and keeping  $x = 0$ ,  $p = 5\%$ ,  $bu = 10$  GWd/tHM) to a few state-of-the-art correlations for  $UO_2$  fuel (i.e., Lucuta [13], Fink [58], MATPRO [21] and Wiesenack [8]). This comparison demonstrates its suitability also to describe  $UO_2$  thermal conductivity.

An independent validation of the new MOX thermal conductivity correlations is shown in Figure 9. The sets of experimental data on fast reactor MOX considered for validation, not included in the fitting set, are those reported by Bonnerot (1988) [48] and Inoue (2000) [35]. Bonnerot provides results of measurements at temperatures between 973 and 2473 K of fresh U-Pu mixed oxides, hypo-stoichiometric with O/M ratio between 1.967 and 1.99, with Pu contents from 5 wt.% and  $\sim 30$  wt.% and porosity between  $\sim 3\%$  and  $\sim 9\%$ . Inoue reported older data on fast reactor MOX from Hetzler (1967), Van Craeynest (1968), Laskiewicz (1971), Fukushima (1983), Elbel (1985 and 1988) (normalized to 100% TD), concerning fresh MOX fuel at temperatures between 350 and 2500 K, with Pu content from 20 to 25 wt.%, O/M ratio from 1.96 to 1.99. The cloud of points mostly lays in a 30% deviation band with respect to the experimental values, with a significant amount of predictions inside the 10% deviation region (corresponding to the best experimental uncertainty on fresh MOX thermal conductivity, from recent works [23], [24]). The largest over-estimations of the experimental values (more than 30%) are observed for the lowest temperatures of the datasets, i.e., close to 500 K, which is the lower limit of validity of the thermal conductivity correlation proposed and below the commercial range of interest for FBR MOX fuels. On the contrary, the agreement with data measured at high temperatures (above 1600 K), representative of the operative conditions of future fast reactors, is remarkably good. The maximum calculated deviation is  $\sim 20\%$  compared to the experimental values. An independent validation against thermal conductivity data on irradiated fast reactor MOX could not

be performed, since there is no other data available in the open literature than those used for the fit [9], [37]. Figure 10 shows the distribution of the relative differences between the values yielded by the MOX thermal conductivity correlation and the experimental data from Bonnerot [48] and Inoue [35]. For most of the correlation predictions (~ 60% and ~ 90% of the Bonnerot and Inoue datasets, respectively), the relative error with respect to the experimental data is below 20%, hence comparable with the state-of-the-art experimental uncertainty on MOX thermal conductivity (reported between 10 and 20% of the measured value, as previously mentioned). The largest deviations are observed for the lower temperature values (between 350 and 1200 K) and correspond to the points outside the 30% deviation band in Figure 9.

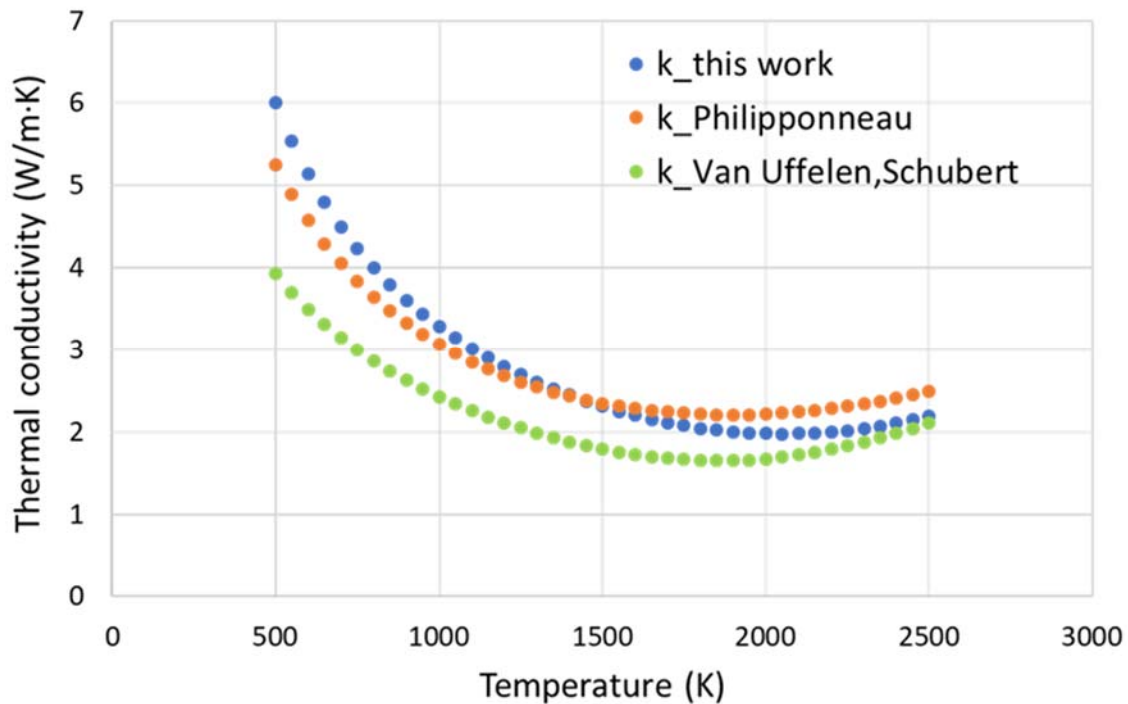


Figure 7: Temperature behaviour of the new MOX thermal conductivity correlation (blue dots), compared to the main state-of-the-art correlations for MOX fuel (Philipponneau [18] and Van Uffelen-Schubert [10]). These values refer to stoichiometric MOX, i.e.,  $x = 0$ , with 20 at.% initial Pu content and 5% porosity, at 10 GWd/tHM burnup.

	Philipponneau [44]	Van Uffelen - Schubert [10]	This work
<b>Root mean square error (rmse)</b>	0.33	0.34	0.16

Table 8: Root mean square error of the MOX thermal conductivity correlation developed in this work, compared to the main state-of-the-art correlations for MOX fuel, over the entire set of data considered in this work (both fresh and irradiated MOX, Table 5).

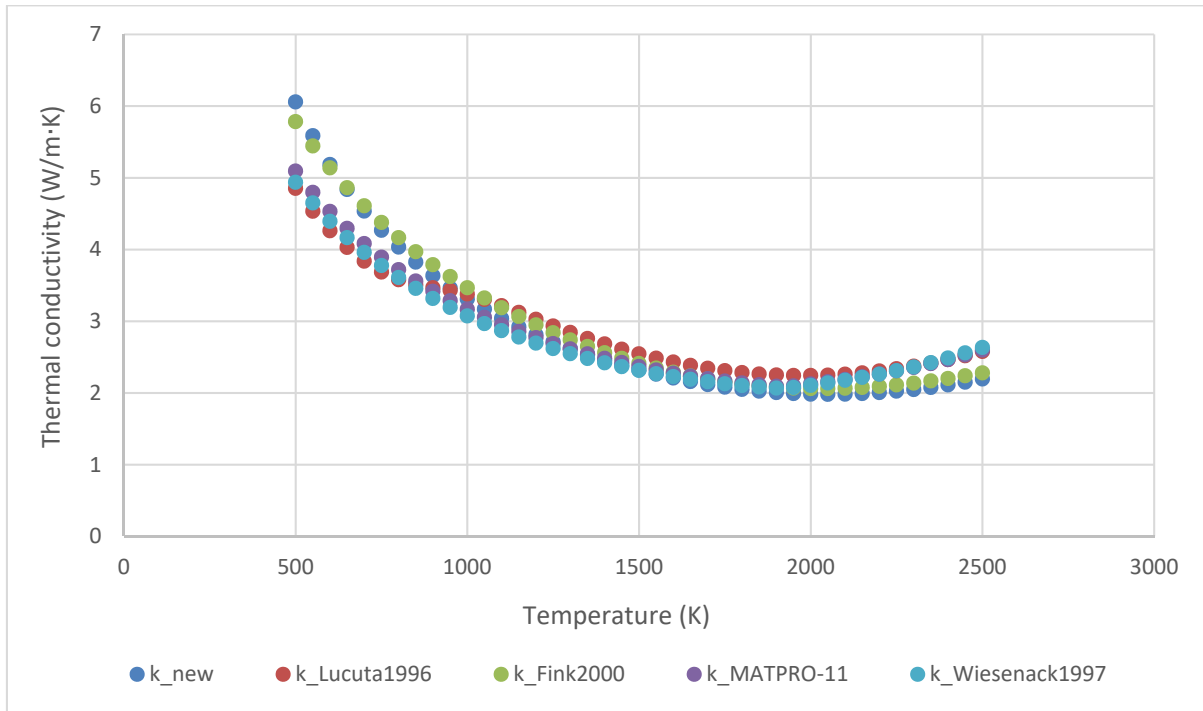


Figure 8: Temperature behaviour of the new MOX thermal conductivity correlation (blue dots), setting zero initial plutonium content, compared to some main state-of-the-art correlations for  $UO_2$  fuel (Lucuta [13], Fink [58], MATPRO [21] and Wiesenack [8]). These values refer to stoichiometric MOX, i.e.,  $x = 0$ , with 5 % porosity, at 10 GWd/tHM burnup.

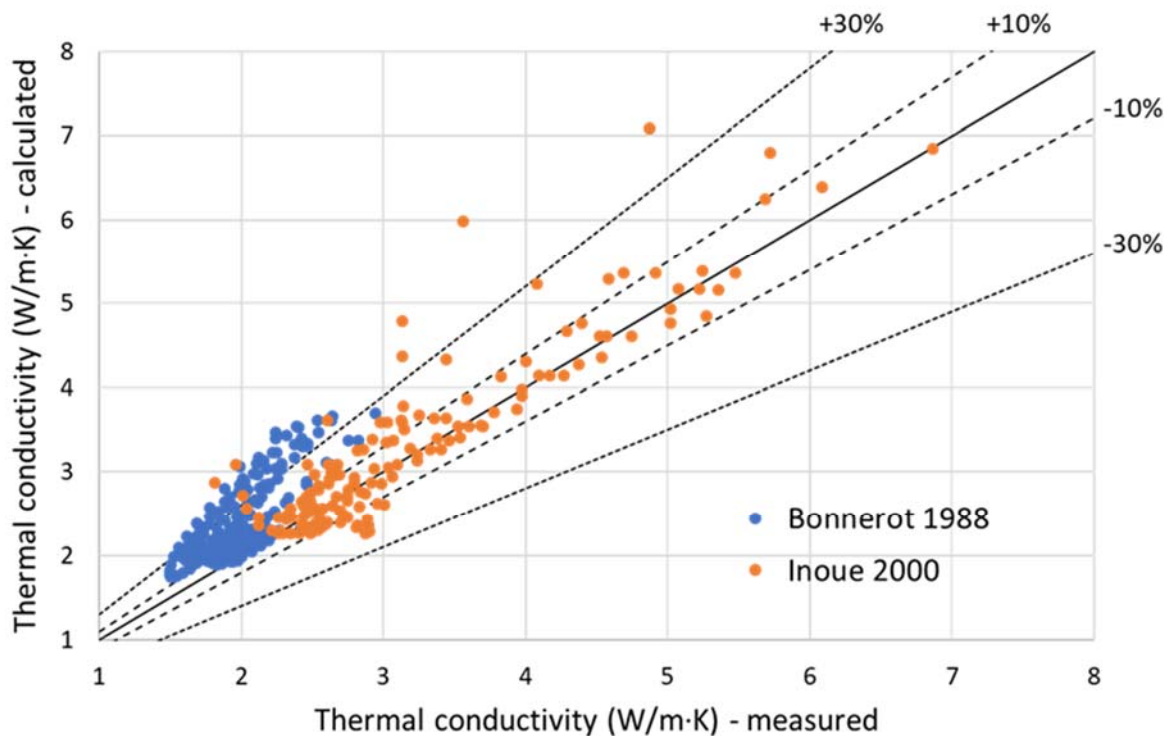


Figure 9: Validation of the thermal conductivity correlation developed in this work against experimental data on fresh MOX, from Bonnerot [48] and reported by Inoue [35].

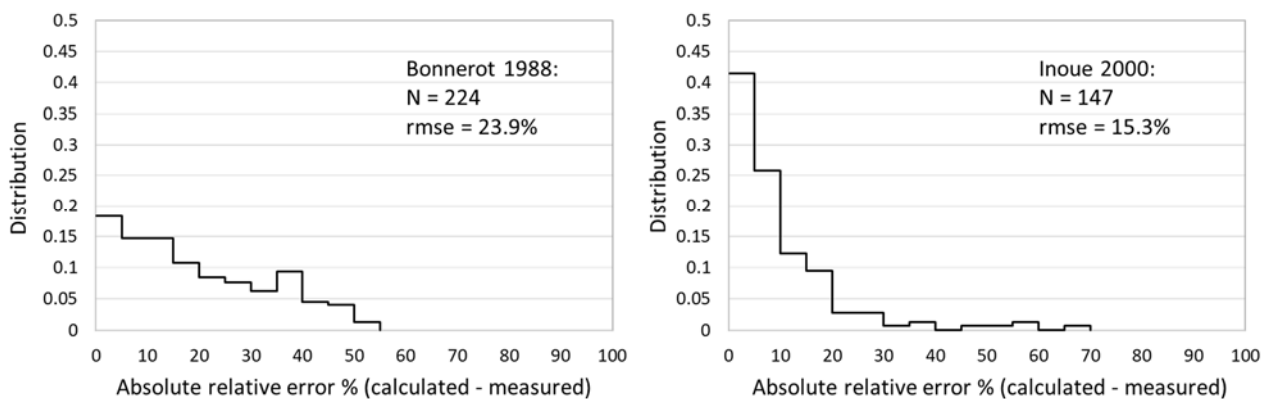


Figure 10: Distribution of the relative differences between calculated values (from the MOX thermal conductivity correlation developed in this work) and experimental data from Bonnerot ([48], left) and Inoue ([35], right). The figure also reports the number of data points analysed and the root mean square error (rmse) of the correlation compared to the two experimental datasets.

## 2.2 Improved model for MOX fuel melting temperature

Among all the available state-of-the-art experimental measurements of MOX melting temperature collected in Table 4, the most recent data obtained through reliable experimental techniques (i.e., laser heating and thermal arrest in rhenium-coated tungsten capsule) were selected as fitting dataset for the new melting temperature correlation. Data measured on samples melted inside a tungsten capsule were excluded due to the confirmed strong contamination by W of the melted fuel material, which affects heavily the melting temperature measured [38], [40]. Moreover, data concerning MOX fuel for fast reactor applications were considered, allowing to cover wide ranges of plutonium contents and deviations from stoichiometry (in the hypo-stoichiometric range). The best (most accurate) experimental data concerning both fresh and irradiated MOX fuel used for the fitting procedure leading to the new correlation are recalled in Table 9.

Fresh MOX data from [29] and [41] corresponding to very high plutonium contents (> 50 wt.%) or to strong hypo-stoichiometry (around 1.90) were excluded from the fitting dataset, since they are out of the range of interest of the present work (i.e., plutonium content up to 50 wt.% and deviation from stoichiometry up to 0.06). The only suitable data about irradiated fast reactor MOX are provided by Konno and Hirosawa [32], who report the actual values of stoichiometry and plutonium content at the sample burnup. Other works on irradiated MOX melting point only report the characteristics of the fresh as fabricated MOX samples [9], [39], [42]. For this reason, the new burnup dependent correlation for the irradiated MOX melting point was fitted on Konno and Hirosawa's data.

Konno *et al.* also developed the most complete MOX melting point correlation available in literature, which includes all the fundamental dependencies of interest, i.e., burnup, stoichiometry, plutonium (and americium) content. This correlation, however, includes mixed-effect terms, which does not allow to evaluate the impact of the single effects on the melting temperature, and is derived based only on own data, measured on MOX fuels irradiated in the JOYO Japanese reactor [32]. The strategy adopted here is similar to that followed to build the new MOX thermal conductivity correlation (see Section 2.1). A correlation describing the melting behaviour of fresh MOX fuel was derived ( $T_{m,0}$ ) and then inserted in a burnup dependent function accounting for the irradiation effects ( $T_{m,irr}$ ). Previous experimental studies showed that both the plutonium content (at least up to 50 wt.%) and the deviation from stoichiometry decrease the MOX melting temperature with respect to fresh, stoichiometric  $UO_2$  [17], [21], [32], [39]. A recent theoretical analysis based on molecular dynamics calculations confirms this effect of plutonium content in mixed oxides [59].

Fresh MOX fuel		
Reference	Measured fuel	Experimental technique
<b>Kato <i>et al.</i>, 2008 (a)</b> [40]	Fresh MOX, O/M = 2.000, Pu content from 29.7 to 46.3 mol%, Am content from 0.3 to 3.3 mol%	Sample heating in a Re capsule, analysis of pyrometer thermograms
<b>Hirosawa <i>et al.</i>, 2011</b> [42]	Fresh FR MOX with O/M = 1.99, Pu content = 31.8 mol%	Sample heating in an inner Re capsule + outer W capsule, Thermal Arrest technique
<b>Bohler <i>et al.</i>, 2014</b> [29]	Fresh MOX, O/M = 2.00, Pu content from 3.7 to 50 mol%	Laser Heating and analysis of pyrometer thermograms
<b>Prieur <i>et al.</i>, 2015</b> [43]	Fresh MOX, O/M = 1.98, Pu content = 22 mol%, Am content = 3.5 mol%	Laser Heating and analysis of pyrometer thermograms
<b>Strach <i>et al.</i>, 2016</b> [30]	Fresh MOX, O/M = 2.00, Pu content from 14 to 54 wt%	Thermal Arrest technique on samples obtained from UO <sub>2</sub> and PuO <sub>2</sub> powders. Measurements in Ar atmosphere
<b>ESNII+ D7.41, 2017</b> [23]	Fresh PHENIX MOX, 95% TD, Pu content 24 mol%, O/M = 2.00 (stoichiometric) and 1.978 (hypo)	Laser Heating and fast multi-channel pyrometry
Irradiated MOX fuel		
Reference	Measured fuel	Experimental technique
<b>Konno, Hirosawa, 2002</b> [32] ( <b>reports also data by Tachibana <i>et al.</i> 1985 and Komatsu <i>et al.</i> 1988</b> )	Irradiated MOX with burnup between 8.2 and 110.9 GWd/tHM, O/M = 1.98, Pu content = 17.5 mol%, Am content = 0.13 mol%	Thermal Arrest technique on sample in a W capsule

Table 9: List of selected experimental data of fresh and irradiated MOX melting point, together with the characteristics about the fuel and the experimental technique employed.

In view of the limited set of available experimental data, the following assumptions were made: (i) a linear dependency on each parameter known to affect (decrease) the melting temperature is assumed, and (ii) each effect is considered to be independent (i.e., additive to each other). Hence, fresh MOX melting point experimental data, reported in Table 9, were initially fitted with the starting function as follows:

$$T_{m,0}([Pu], [Am], x) = T_{m,UO_2} - \gamma_{Pu} [Pu] - \gamma_{Am} [Am] - \gamma_x x \quad (4)$$

Where,  $T_{m,UO_2}$  is the fresh UO<sub>2</sub> melting temperature, i.e., 3147 K according to recent and reliable experimental measurements by Manara *et al.* [60], recommended by the ESNII+ Catalogue on MOX properties [31];  $[Pu]$  and  $[Am]$  are the plutonium and americium contents, respectively (both in at./),  $x$  is the deviation from stoichiometry.  $\gamma_{Pu}$ ,  $\gamma_{Am}$ ,  $\gamma_x$  are the regressors associated to each effect to be fitted on the selected fresh MOX melting temperature data. An effect of the americium content is initially considered since some of the works considered include data on Am-bearing MOX fuel ([39], [40], [43], from Table 9), which is of interest for Generation IV type of fuels. The functional form proposed for  $T_{m,0}$  relies on the fact that each of the parameters causes a decrease of the MOX melting point with respect to fresh stoichiometric UO<sub>2</sub> [17], [21], [32], [39].

Following the same strategy adopted for the fresh MOX thermal conductivity, a statistical analysis based on the p-values was performed (again using the R statistical code), assuming a threshold p-value of 5% for the significance of the regressors in the proposed correlation. From the analysis of the p-values, it can be inferred that the effect of plutonium content and stoichiometry should be included in the fresh MOX melting temperature correlation, since the p-values associated to their regressors are very low, both from the fit on the whole set of data ( $\sim 10^{-13}$  and 1.3%, respectively) and from the fit on the subset

of only Pu and x-dependent data ( $\sim 10^{-7}$  and 4.7%, respectively). On the contrary, the analysis suggests excluding the Am-dependent term from the correlation, as its p-value is greater than 5 % also from the fit over the subset of Am-dependent data (20%). Most of the available data on fresh MOX melting point are about (U,Pu)O<sub>2-x</sub> fuel, while only few samples of the database include Am, and with an extremely low americium content ( $< 4$  wt.%)<sup>3</sup>. Therefore, the available dataset considered here is not representative of the americium effect on the fresh MOX melting temperature, which will be treated in the next INSPYRE Deliverable of Task 6.3, D6.5.

As a result of the statistical analysis, the form proposed for the fresh MOX melting temperature correlation is as follows:

$$T_{m,0}([Pu], x) = T_{m,UO_2} - \gamma_{Pu} [Pu] - \gamma_x x \quad (5)$$

The final fit of Eq. 5 over the complete set of fresh MOX melting temperature data (Table 9) yields the results summarized in Table 10, in terms of regressor values. The reported values for the fit coefficients hold for  $T_{m,UO_2}$  expressed in K and plutonium concentration  $[Pu]$  expressed in at./  $T_{m,0}$  is calculated in K. The analysis of the residual trends (not shown here, for sake of brevity) does not suggest the need of the introduction of higher order or mixed terms (present in the correlation by Konno *et al.*, which involves, e.g., a squared dependence on the plutonium content [32]), since the fit residuals are randomly distributed if plotted against  $[Pu]$ ,  $[Am]$  or x. The comparison between the experimental data and the corresponding values predicted by the new fresh MOX melting temperature correlation is shown in Figure 11.

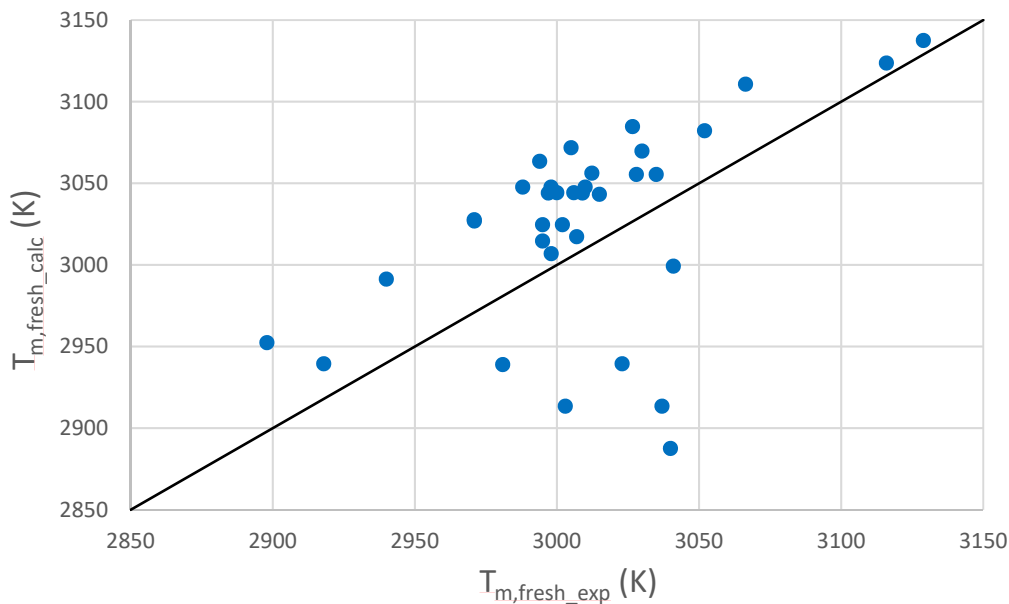


Figure 11: Comparison between the fresh MOX melting temperature data (Table 9) and the corresponding predictions given by the correlation fitted on these data (Eq. 5).

Regressor	Units	Estimate
$\gamma_{Pu}$	K/at./	364.85
$\gamma_x$	K	1014.15

Table 10: Results of the fit of the statistically assessed  $T_{m,0}([Pu], x)$  correlation (Eq. 5) on the whole set of the selected fresh MOX melting temperature data.

<sup>3</sup> The effect of Am is represented in the Konno et al. correlation [32] based on the ideal solution model and obtained performing experimental regression analysis under the hypothesis of additive effects.

Figure 11 shows that the agreement between the experimental and fitted melting temperature values is acceptable, despite some deviations up to 50 K. The maximum residual, however, is comparable with the high experimental uncertainty on MOX melting point, which is between 30 and 70 K [23], [28], [29], [41], [42].

Once the correlation for fresh MOX melting temperature,  $T_{m,0}([Pu], x)$ , is obtained (Eq. 5, with regressor values in Table 10), the correlation for irradiated MOX melting temperature is derived by fitting the selected data on irradiated fuel reported in Table 9 [32]. According to experimental results, irradiation degrades MOX fuel melting point with respect to fresh MOX [32], [39], [42]. To account for the burnup effect, an exponential functional form is again adopted. This was chosen because the effect of burnup reflects the continuous build-up of defects and fission products, which evolves towards saturation [39], and recent molecular dynamics calculations of the melting temperature in mixed oxides [59] suggest a decrease of the melting temperature when a few atom percent of foreign atoms are introduced in the lattice. This was ascribed to a decreasing Frenkel formation energy in MOX caused by a lattice mismatch induced by a small quantity of foreign atoms (up to a few percent). The burnup range considered in this work is of the order of the atom percent (up to  $\sim 110$  GWd/tHM), hence the functional form chosen for the irradiated MOX melting temperature correlation is

$$T_{m,irr}(bu, [Pu], x) = T_{m,inf} + (T_{m,0}([Pu], x) - T_{m,inf}) \cdot e^{-\frac{bu}{\delta}} \quad (6)$$

Where,  $bu$  is the fuel burnup in GWd/tHM,  $T_{m,0}([Pu], x)$  is the melting temperature of the fresh fuel according to Eq. 5, while  $T_{m,inf}$  and  $\delta$  are the correlation parameters to be fitted on the set of irradiated MOX melting temperature data. This formulation is consistent with  $T_{m,irr}(bu, [Pu], x) = T_{m,0}([Pu], x)$  when the fuel burnup is equal to zero. Fitting this functional form to the irradiated MOX data collected in Table 9 leads to the fit regressor values reported in Table 11. The comparison between the values predicted by the new correlation (Eq. 6) and the corresponding experimental values is shown in Figure 12. The average deviation from the experimental data is around 15 K, consistent with the experimental uncertainty reported for irradiated MOX melting temperature (between 10 and 30 K) [32]. The agreement between the calculated and measured values is even better when considering the experimental uncertainties, as most of the error bars reported in Figure 12 include the perfect agreement represented by the plot diagonal.

Regressor	Units	Estimate
$T_{m,inf}$	K	2964.92
$\delta$	GWd/tHM	40.43

Table 11: Results of the fit of the  $T_m(bu, [Pu], x)$  correlation (Eq. 6) over the selected irradiated MOX melting temperature data.

The ranges of applicability of the newly developed correlations for MOX fuel melting temperature, corresponding to the ranges covered by the experimental data considered, are:

- Deviation from stoichiometry,  $x$ : [0, 0.06] (hypo-stoichiometry)
- Plutonium content,  $[Pu]$ : [0, 50] wt.%
- Burnup,  $bu$ : [0, 110] GWd/tHM.

In Figure 13, the behaviour of the new correlation for MOX melting temperature as a function of (a) plutonium content (considering stoichiometric fuel at 10 GWd/tHM) and (b) fuel burnup (considering stoichiometric fuel with 30 wt.% initial Pu content) is compared with two state-of-the-art correlations, Konno *et al.* [32] and MATPRO ([21], valid for  $UO_2$  and LWR MOX).

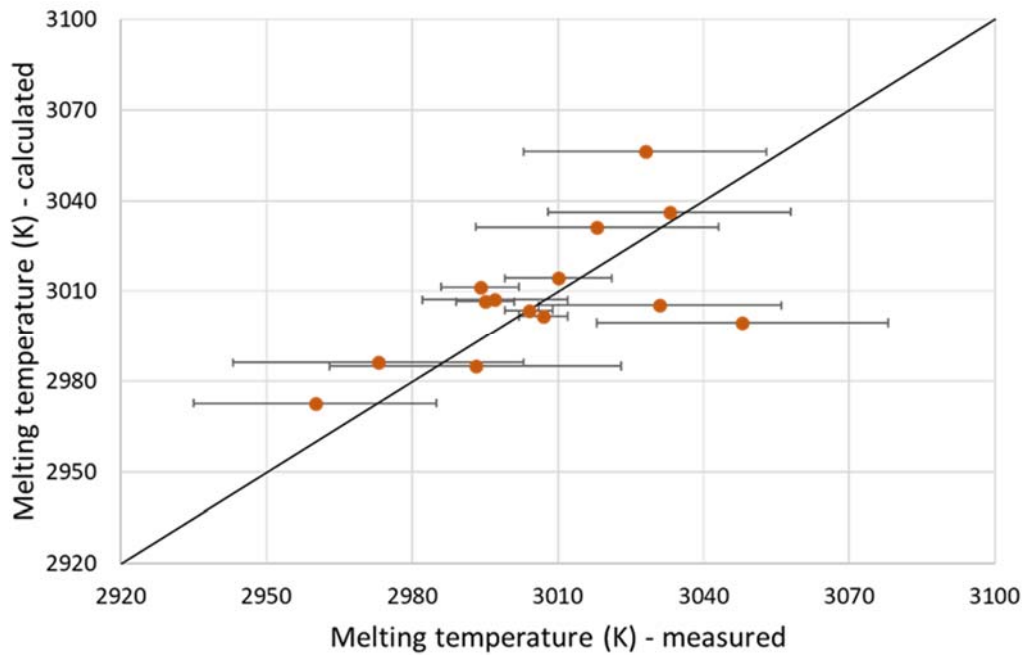


Figure 12: Comparison between the irradiated MOX melting point data (Table 9) and the corresponding predictions given by the correlation fitted on these data (Eq. 6). The experimental uncertainties, as provided by the original references [27], [32], [38], are included as horizontal error bars.

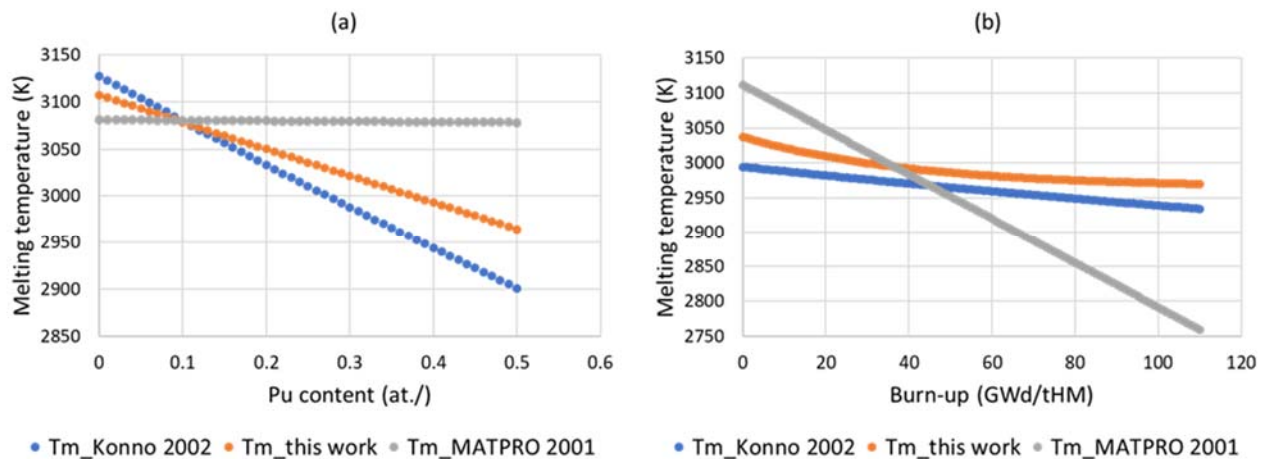


Figure 13: Behaviour of the new MOX melting temperature correlation (blue dots), as a function of (a) Pu content and (b) burnup, compared to two main state-of-the-art correlations for MOX fuel (Konno [32] and MATPRO [21]). These values, in both graphs, refer to stoichiometric MOX, i.e.,  $x = 0$ , while in (a)  $bu = 10$  GWd/tHM and in (b)  $[Pu] = 30$  at.%.

As can be seen in Figure 13, the two current correlations considered for comparison predict sensibly different behaviours and with values predicted that differ by more than 100 degrees. The new correlation for  $T_{m,irr}$  provides values between the two state-of-the-art correlations. The effect of plutonium is negligible in the MATPRO correlation, while in the one by Konno *et al.* a stronger degradation of the predicted melting temperature is observed with increasing plutonium content (at 10 GWd/tHM burnup, as showcased in Figure 13a). This could be due to the fact that the plutonium content effect in the Konno *et al.* correlation [32] is based on quite old and low in value (down to 2850 K at 50 at.% Pu) experimental data on MOX fuels, provided by Lyon and Baily [25] and Aitken and Evans [26]. The burnup effect is derived by Konno by fitting Japanese experimental data from JOYO reactor campaigns reported in his same work [32]. The novel correlation proposed, instead, is based on a wider

dataset, composed of recent and up-to-date literature works from various authors (including Konno's data for the burnup effect), showing experimental data of MOX melting temperature which are higher in value (never lower than 2950 K, as shown in Figures 11 and 12). Moreover, it exhibits an exponential decreasing trend in burnup, which leads to higher melting temperature value at high burnup. This could be due to the fact that, at such burnup values, either the high burnup structure formation in the low temperature fuel region is accompanied by a reduction of the fission products in the lattice (observed using EPMA [61]–[63]), or a large fractional release of fission products occurs in FBR MOX fuels in the high temperature region.

Table 12 reports the root mean square errors of the three correlations considered compared to the set of available experimental data, both on fresh and irradiated MOX fuel (Table 9). The error of the correlation developed in this work is much lower than half the error of the two main state-of-the-art correlations [21], [32] over the considered data.

	Konno et al. [32]	MATPRO [21]	This work
Root mean square error (rmse)	0.014	0.029	0.0065

Table 12: Root mean square error of the MOX melting temperature correlation developed in this work, compared to the main state-of-the-art correlations for MOX fuel, over the entire set of available data on fresh and irradiated MOX (Table 9).

Figure 14 shows the behaviour of the new correlation concerning the degradation of the melting temperature of  $\text{UO}_2$  fuel with burnup (setting  $[\text{Pu}] = 0$  in the new correlation and considering stoichiometric  $\text{UO}_2$ ).

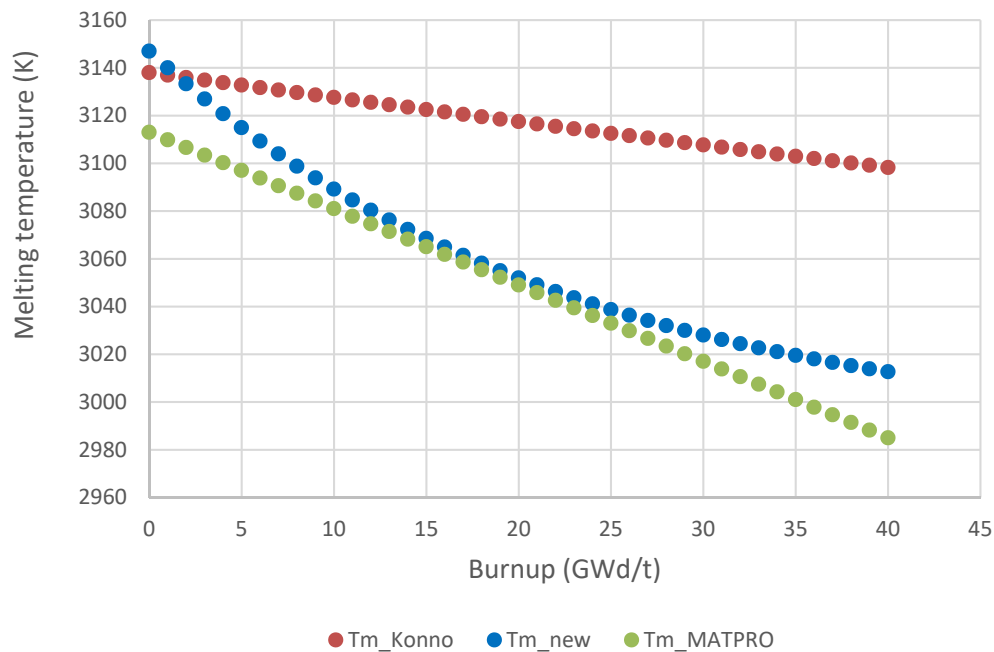


Figure 14: Burnup behaviour of the new MOX melting temperature correlation (blue dots), setting zero initial plutonium content, compared to the two main state-of-the-art correlations applied to  $\text{UO}_2$  fuel (Konno et al. [32] and MATPRO [21], with  $[\text{Pu}] = 0$ ). These values refer to stoichiometric fuel ( $x = 0$ ).

Starting from 3147 K (i.e.,  $\text{UO}_2$  melting point according to Manara *et al.* [60]), the melting temperature yielded by the new correlation decreases significantly faster than those obtained by Konno's correlation, which is also specifically conceived for FR MOX fuel, but proves itself not applicable to  $\text{UO}_2$  fuel. On the contrary, the new  $T_{m,irr}$  correlation, if applied to  $\text{UO}_2$ , shows a burnup behaviour in agreement with the MATPRO one (specifically developed for  $\text{UO}_2$  fuel), with acceptable deviations at low and high burnup.

### 3 JOINT OXYDE-GAINE (JOG): STATE OF THE ART AND ISSUES

At the beginning of irradiation, a free space (the rod gap) is left between the fuel pellets and the surrounding cladding material to accommodate the volume changes of both the fuel and cladding, caused in particular by swelling and creep. The gap in fresh fuel rods is filled with helium gas, but this composition gradually changes as a result of fission gas release during irradiation. In FR fuel rods, the irradiation conditions (in terms of power and fuel temperature) are such that, at higher burnups, the gap can become filled with the so-called JOG (Joint Oxyde-Gaine), a layer consisting of fission product compounds [64]. This layer has been observed as a result of PIEs (i.e., X-ray images by EPMA) on MOX fuel samples irradiated in fast reactor conditions in the EBR-II, Rapsodie and Phenix (NESTOR experiments) reactors [65]. The JOG impacts on the heat transfer from the fuel towards the cladding and then the coolant, since the release and accumulation of fission products and their compounds in the gap modifies the gap conductance, supposedly improving it (with respect to the gaseous open gap) and being beneficial in terms of fuel temperature regime [20]. Moreover, the JOG formation has an influence also on the mechanical and chemical pin performance. Indeed, it drives the evolution of the fuel radial deformation (i.e., fuel swelling, especially at high burnup) and the gap dynamics [66], while the fission products in the JOG play a predominant role on Fuel-Cladding Chemical Interaction (FCCI) and on the resulting strong corrosion of the inner cladding surface [67].

The knowledge about JOG formation and properties is currently limited [68], essentially because of the scarcity of direct experimental measurements of the JOG available in the open literature [69]. Some experimental and theoretical investigations contributed to gain better understanding of the JOG formation. The volatile fission products (Cs, Te, I), which are produced and accumulate in MOX fuel during irradiation, have no stable compounds allowing them to remain in the hot regions of the pellets [67]. Above a threshold temperature of about 1200°C, they behave like fission gases (Xe and Kr), i.e., they migrate radially down the thermal gradient and condensate in the colder fuel region at the periphery of the fuel pellets. Radial migration concerns not only the volatile fission products, but also some other fission products with high vapour pressure or that may form compounds with high vapour pressures. For example, at high burnup, when oxide fuel reaches high oxygen potential, molybdenum transforms into oxidized forms, and some of the compounds formed (especially  $\text{Cs}_2\text{MoO}_4$  and  $\text{MoO}_3$ ) have high vapour pressure, which explains how Mo migrates towards the pellet periphery. From the fuel outer surface, they can be released in the gap between the fuel and the cladding, where they form a bonding layer, typically called JOG. It starts to form at the interface fuel-cladding at intermediate burnups, first at the peak power node (where fuel temperature is higher and radial migration is enhanced), typically after gap closure, in the residual space left due to surface roughness [67]. As for the evolution of the JOG, the governing mechanisms are still unknown and currently under investigation, and a physical explanation is far from being assessed. At high burnup the JOG can reach (as experimentally observed) a diameter width up to 150  $\mu\text{m}$  in unstrained pins, and even larger diameters, up to 300  $\mu\text{m}$ , in pins with high swelling claddings [64], [70], [71].

Atomic scale calculations and fuel chemistry codes (Gibbs energy minimizers e.g., CALPHAD) provide indications about the composition of the JOG layer [72]–[75]. The elements and compounds predicted to be present in the JOG phase are Te, CsI,  $\text{Cs}_2\text{Te}$ ,  $\text{Cs}_3\text{Te}_2$ ,  $\text{Cs}_2\text{MoO}_4$  [72], [73]. From EPMA experimental investigations reported by [67], [72], the JOG layer is predominantly composed by the elements molybdenum, caesium, oxygen, while tellurium and other fission products are observed in smaller quantities. If the JOG is well defined, uranium and plutonium are not detected inside it. Additionally, some cladding elements and their oxides, e.g.,  $\text{Cr}_2\text{O}_3$  and  $\text{CrMoO}_4$ , might be present, especially if some cladding corrosion has taken place, since oxygen tends to associate with the chromium present in the cladding. Among these compounds,  $\text{Cs}_2\text{MoO}_4$  is considered the prevalent and most important one in

determining the JOG properties. Cs is heavily released in the fuel-cladding gap (~ 70-80% of the Cs produced) after a strong radial migration, and  $\text{Cs}_2\text{MoO}_4$  is the stable Cs compound at high temperatures and high burnups [72]. The exact composition of the JOG phase, however, is still not well known, and it varies both axially and azimuthally depending on local fuel temperature, oxygen potential and piling-up of fission products after radial and axial migration.

There is only limited knowledge on the heat transfer properties of the JOG. The thermal conductivity of caesium molybdate  $\text{Cs}_2\text{MoO}_4$ , which is supposed to be the main constituent of the JOG, was measured by the laser-flash method and lies in the range  $0.3\text{--}0.5 \text{ W m}^{-1} \text{ K}^{-1}$ , at fast reactor operating temperatures [76], [77]. This value is 5–10 times lower than the  $(\text{U,Pu})\text{O}_2$  thermal conductivity, but much higher than the xenon and rod filling gas thermal conductivity. Therefore, the heat transfer between fuel and cladding is much better through the JOG layer than through an equivalent depth filled with fission gases, although not as good as in case of a closed gap, when the oxide fuel is directly in contact with the cladding.

Furthermore, the JOG layer is probably not completely dense and uniform, because in the hottest regions of the JOG some fission product compounds might migrate, leaving voids that locally deteriorate the heat transfer properties. From the pin geometry point of view, the JOG formation is associated with a decrease of the pellet diameter, especially in pins with low-swelling steel cladding. The release outside the oxide matrix of a considerable fraction of fission products induces a sharp decrease of the matrix swelling [78], and consequently a decrease of the pellet diameter, giving space for JOG to form between fuel outer and cladding inner surfaces.

The formation and evolution of the JOG layer clearly impacts the thermal, chemical and mechanical performance of fast reactor fuel pins. For example, the fuel central temperature in fast reactor conditions is surely affected by the JOG thermal conductivity contribution and its heat transfer properties, which are currently highly uncertain (as pointed out in the ESFR-SMART project of the EU [79]). Hence, it is important to implement a model able to evaluate the JOG formation and evolution during irradiation in fast reactor conditions in fuel performance codes.

Various approaches are adopted in the fuel performance codes for FR fuels. Some of them disregard the formation of an outer fuel compound entirely (e.g. FRED, TRANSURANUS, TRAFIC, SIM, FEMAXI-FBR, BERKUT), while others model its formation in a purely empirical manner as a function of temperature and/or burnup (e.g. CEPTAR) [79]. Only a few codes consider the direct migration of individual fission products like Cs and the resulting compound formation. One example is the FEAST-OXIDE code developed at MIT [80], [81], although they do not consider the details of the fuel thermo-chemistry. A more complete approach is being implemented in the CEDAR and GERMINAL codes. These FPCs are coupled with a thermo-chemistry code able to predict the stable compounds constituting the JOG, e.g., ANGE, a Gibbs energy minimizer coupled with the GERMINAL FPC [73]. The fission product release in the rod gap and the temperature calculated by the FPC are provided as inputs to the thermo-chemistry module, which yields the chemical composition of the gap and some estimated properties (e.g., the species melting point), which are returned back to the FPC.

The two main parameters representative of the JOG in FPCs are the JOG volume (thickness) and thermal conductivity. The main issue related to an accurate JOG model is that the overall JOG composition must be provided as input to calculate any of its thermodynamic properties. Moreover, knowing the irradiation conditions and the concentration of species released in the gap, thermodynamic calculations can provide the enthalpy of formation of phases in the rod gap, but no thermal conductivity information. It is worth pointing out that some data have recently been published on the density of some compounds as a function of the temperature [82].

From the computational point of view, among the codes used in the INSPIRE project, only the GERMINAL FPC [83] currently includes modelling of JOG evolution. Two different JOG models and approaches are implemented in GERMINAL:

- An empirical model able to estimate the JOG thickness, as a function of burnup, from the caesium released in the fuel-cladding gap (neglecting axial migration, relying on some simplifying hypotheses on the JOG composition and thermal conductivity);
- A coupled approach, consisting in GERMINAL coupled with CALPHAD thermodynamic and thermochemical calculations (proprietary of CEA, not publicly available).

Given the current lack of useful experimental data about JOG, the approach pursued in the INSPYRE Project is schematically shown in Figure 15. It is similar to the approach adopted for the CEDAR code, which is coupled with the MINERVA code for chemical equilibrium calculations [84]. It consists in estimating the JOG composition (as a result of fission product radial migration and release from the fuel) exploiting the current capabilities of the GERMINAL FPC [83], and with this input, run CALPHAD calculations to evaluate thermodynamic data on the phases that are supposed to form the JOG in the fuel-cladding gap (Task 4.1). As a complement, the TRANSURANUS FPC [10] is being coupled with the SCIANTIX [85] and MFPR-F [86] codes, working at the fuel grain level and able to accurately simulate the fission product migration in the fuel towards the fuel-cladding gap, as well as their release. In addition to this, thermochemical capabilities and a model for the axial migration of fission products in the gap are under development in TRANSURANUS, allowing for a better understanding, description and independent validation of the gap behaviour and JOG during irradiation. Once new experimental data and simulation results are yielded by the activities of Tasks 1.1 and 4.1, a preliminary simple model could be built and implemented in European FPCs, which would be a significant improvement with respect to the current FPC versions (target of Task 7.1). The outcome of this approach will be presented in the D6.5 Deliverable.

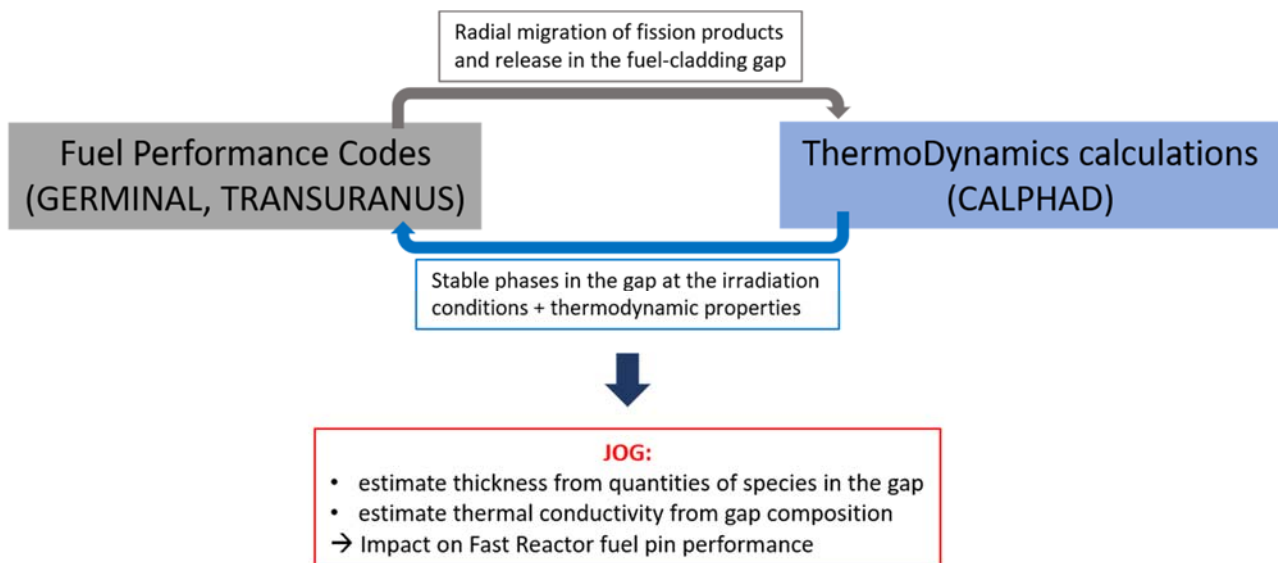


Figure 15: Proposed methodology to develop a model for JOG formation and evolution that would be implemented in fuel performance codes in the INSPYRE Project.

The JOG formation and behaviour in FBR pins under irradiation remains an important issue that needs to be better understood and better modelled in fuel performance codes. It is a complex and challenging topic since few experimental results are available and since the JOG mechanisms involve not only thermodynamics, but also considerable radial and axial migration of a great number of fission products and of their compounds.

## 4 CONCLUSION AND FUTURE DEVELOPMENTS

The aim of this deliverable was to obtain new, accurate, physically grounded models for  $(U,Pu)O_{2-x}$  MOX fuel thermal conductivity and melting temperature, inclusive of all the fundamental effects (i.e., fuel temperature, burnup, stoichiometry, plutonium content, porosity).

The first step consisted in collecting and revising existing correlations for MOX thermal conductivity and melting point, which are implemented in fuel performance codes or available in the open literature, spanning from the '70s up to recent years. The whole set of correlations, both for the effective thermal conductivity ( $k_{eff}$ ) and the melting temperature ( $T_m$ ) (especially concerning homogeneous MOX, according to the Gen-IV strategy), has been classified according to the considered dependencies. This analysis showed the lack of important effects in state-of-the-art correlations, e.g., the initial MOX plutonium content. The plots of  $k_{eff}(T, bu)$  and  $T_m(bu, [Pu])$ , together with the associated relative spread on the average values, helped to identify the most uncertain temperature and burnup regions, which need to be further investigated. A wide set of experimental measurements of thermal conductivity and melting temperature of MOX fuel, published in the open literature, as well as the recent results obtained in the framework of the recent ESNII+ Project (2017), was also collected. This complete database is the necessary starting point for the development and assessment of improved correlations suitable to determine the thermal properties of both fresh and irradiated MOX.

New correlations were built on a physical basis and fitted on the most recent and reliable experimental measurements. The new correlations consider all the fundamental parameters influencing the MOX thermal conductivity (i.e., temperature, stoichiometry, plutonium content, porosity and burnup) and the MOX melting point (i.e., stoichiometry, plutonium and americium contents, burnup). Moreover, they were both statistically assessed on the base of the regressor p-values, to derive a final formulation including only the significant regressors, discarding the effects not represented by the considered experimental dataset. The values predicted by the new correlations are in good agreement with the experimental measurements (considering the reported experimental uncertainties), proving the quality of the approach and of the nature of the correlations developed in this work, which represent a step forward with respect to the state of the art.

New MOX thermal conductivity and melting point measurements would improve and further validate the proposed correlations, extending their validation range. In particular, the analysis presented here suggests that further investigations of the impact of the deviation from stoichiometry and plutonium content on the MOX fuel thermal conductivity are necessary. Additional accurate data would help to better evaluate these two effects which are still controversial. Moreover, measurements on Am- and Np-bearing MOX samples are of great interest to allow the inclusion of the effect of the minor actinides americium and neptunium (which cannot be assessed through the available data collected here) on the thermal conductivity and melting temperature correlations, extending the herein developed ones.

This work contributes to the ongoing development of the European fuel performance codes (GERMINAL, MACROS, TRANSURANUS), objective of Task 7.1 of INSPIRE. The next step will be the implementation of these new MOX thermal conductivity and melting point models in current FPCs and their assessment against both local (separate effect) and integral (on the fuel rod scale) experimental data.

## REFERENCES

- [1] C. Cozzo, D. Staicu, J. Somers, A. Fernandez, and R. J. M. Konings, “Thermal diffusivity and conductivity of thorium-plutonium mixed oxides”, *J. Nucl. Mater.*, vol. 416, no. 1–2, pp. 135–141, 2011.
- [2] M. Saoudi *et al.*, “Thermal diffusivity and conductivity of thorium- uranium mixed oxides”, *J. Nucl. Mater.*, vol. 500, pp. 381–388, 2018.
- [3] D. Jain, C. G. S. Pillai, B. S. Rao, R. V. Kulkarni, E. Ramdasan, and K. C. Sahoo, “Thermal diffusivity and thermal conductivity of thoria-lanthana solid solutions up to 10 mol.% LaO<sub>1.5</sub>”, *J. Nucl. Mater.*, vol. 353, no. 1–2, pp. 35–41, 2006.
- [4] D. Staicu *et al.*, “Thermal conductivity of homogeneous and heterogeneous MOX fuel with up to 44 MWd/kgHM burnup”, *J. Nucl. Mater.*, vol. 412, no. 1, pp. 129–137, 2011.
- [5] D. Staicu and M. Barker, “Thermal conductivity of heterogeneous LWR MOX fuels”, *J. Nucl. Mater.*, vol. 442, no. 1–3, pp. 46–52, 2013.
- [6] N. Nakae *et al.*, “Thermal property change of MOX and UO<sub>2</sub> irradiated up to high burnup of 74 GWd/t”, *J. Nucl. Mater.*, vol. 440, no. 1–3, pp. 515–523, 2013.
- [7] M. Amaya, J. Nakamura, F. Nagase, and T. Fuketa, “Thermal conductivity evaluation of high burnup mixed-oxide (MOX) fuel pellet”, *J. Nucl. Mater.*, vol. 414, no. 2, pp. 303–308, 2011.
- [8] W. Wiesenack, “Assessment of UO<sub>2</sub> Conductivity Degradation Based on In-pile Temperature Data”, in: *ANS International Topical Meeting on LWR Fuel Performance, Portland, Oregon, 1997*, pp. 507–511, 1997.
- [9] K. Yamamoto, T. Hirose, K. Yoshikawa, K. Morozumi, and S. Nomura, “Melting temperature and thermal conductivity of irradiated mixed oxide fuel”, *J. Nucl. Mater.*, vol. 204, no. C, pp. 85–92, 1993.
- [10] European Commission, *TRANSURANUS Handbook*, Joint Research Centre, Karlsruhe, Germany 2018.
- [11] B. Lee, Y. Koo, and D. Sohn, “Modelling of MOX fuel’s thermal conductivity considering its microstructural heterogeneity”, in: *IAEA Technical Committee meeting, Windermere, United Kingdom, 2000*, pp. 247–256, 2000.
- [12] K. J. Geelhood and W. G. Luscher, *FRAPCON-3.5: A Computer Code for the Calculation of Steady-State, Thermal-Mechanical Behavior of Oxide Fuel Rods for High Burnup*, vol. NUREG/CR-7. 2014.
- [13] P. G. Lucuta, H. Matzke, and I. J. Hastings, “A pragmatic approach to modelling thermal conductivity of irradiated UO<sub>2</sub> fuel: Review and recommendations”, *J. Nucl. Mater.*, vol. 232, no. 2–3, pp. 166–180, 1996.
- [14] J. J. Carbajo, G. L. Yoder, S. G. Popov, and V. K. Ivanov, “A review of the thermophysical properties of MOX and UO<sub>2</sub> fuels”, *J. Nucl. Mater.*, vol. 299, no. 3, p. 181, 2001.
- [15] D. G. Martin, “A re-appraisal of the thermal conductivity of UO<sub>2</sub> and mixed (U, Pu) oxide fuels”, *J. Nucl. Mater.*, vol. 110, no. 1, pp. 73–94, 1982.
- [16] L. Luzzi, S. Lorenzi, D. Pizzocri, A. Aly, D. Rozzia, and A. Del Nevo, “Modeling and Analysis of Nuclear Fuel Pin Behavior for Innovative Lead Cooled FBR”, Report RdS/PAR2013/022, 2014.
- [17] K. Lassmann, A. Schubert, P. Van Uffelen, C. Gyori, and J. van de Laar, *TRANSURANUS Handbook, Copyright © 1975-2014*, Karlsruhe, Germany: Institute for Transuranium Elements, 2014.
- [18] Y. Philipponneau, “Thermal conductivity of (U, Pu)O<sub>2-x</sub> mixed oxide fuel”, *J. Nucl. Mater.*, vol. 188, no. C, pp. 194–197, 1992.

- [19] M. Suzuki, H. Saitou, Y. Udagawa, and F. Nagase, *Light Water Reactor Fuel Analysis Code FEMAXI-7; Model and Structure*, July 2013.
- [20] M. Teague, M. Tonks, S. Novascone, and S. Hayes, “Microstructural modeling of thermal conductivity of high burnup mixed oxide fuel”, *J. Nucl. Mater.*, vol. 444, no. 1–3, pp. 161–169, 2014.
- [21] L. J. Siefken, E. W. Coryel, E. A. Harvego, and J. K. Hohorst, *SCDAP/RELAP5/MOD 3.3 Code Manual, MATPRO - A Library of Materials Properties for Light-Water-Reactor Accident Analysis*, vol. 4, 2001.
- [22] M. Kato, K. Maeda, T. Ozawa, M. Kashimura, and Y. Kihara, “Physical properties and irradiation behavior analysis of Np- and Am-Bearing MOX Fuels”, *J. Nucl. Sci. Technol.*, vol. 48, no. 4, pp. 646–653, 2011.
- [23] D. Staicu *et al.*, “Preparing ESNII for HORIZON 2020 - Deliverable D7.4.1 - Measurement of properties of fresh Phenix fuel”, ESNII+ Deliverable, 2017.
- [24] D. Staicu *et al.*, “Preparing ESNII for HORIZON 2020 - Deliverable D7.3.4 - Characterization and measurement of properties of fresh TRABANT fuel”, ESNII+ Deliverable, 2017.
- [25] L. Lyon and E. Baily, “The solid-liquid phase diagram for the  $\text{UO}_2\text{-PuO}_2$ ”, *J. Nucl. Mater.*, vol. 22, no. 10, pp. 332–339, 1967.
- [26] M. G. Adamson, E. A. Aitken, and R. W. Caputi, “Experimental and thermodynamic evaluation of the melting behavior of irradiated oxide fuels”, *J. Nucl. Mater.*, vol. 130, no. C, pp. 349–365, 1985.
- [27] J. Komatsu, T. Tachibana, and K. Konashi, “The melting temperature of irradiated oxide fuel”, *J. Nucl. Mater.*, vol. 154, no. 1, pp. 38–44, 1988.
- [28] F. De Bruycker *et al.*, “On the melting behaviour of uranium/plutonium mixed dioxides with high-Pu content: A laser heating study”, *J. Nucl. Mater.*, vol. 419, no. 1–3, pp. 186–193, 2011.
- [29] R. Böhler *et al.*, “Recent advances in the study of the  $\text{UO}_2\text{-PuO}_2$  phase diagram at high temperatures”, *J. Nucl. Mater.*, vol. 448, no. 1–3, pp. 330–339, 2014.
- [30] M. Strach, D. Manara, R. C. Belin, and J. Rogez, “Melting behavior of mixed U-Pu oxides under oxidizing conditions”, *Nucl. Instruments Methods Phys. Res. Sect. B Beam Interact. with Mater. Atoms*, vol. 374, pp. 125–128, 2016.
- [31] P. Martin *et al.*, “Preparing ESNII for HORIZON 2020 - Deliverable D7.5.1 - Catalog on MOX properties for fast reactors”, ESNII+ Deliverable, 2017.
- [32] K. Konno and T. Hirosawa, “Melting temperature of mixed oxide fuels for fast reactors”, *J. Nucl. Sci. Technol.*, vol. 39, no. 7, pp. 771–777, 2002.
- [33] R. L. Gibby, “The effect of plutonium content on the thermal conductivity of (U, Pu) $\text{O}_2$  solid solutions”, *J. Nucl. Mater.*, vol. 38, pp. 163–177, 1971.
- [34] C. Duriez, J. P. Alessandri, T. Gervais, and Y. Philipponneau, “Thermal conductivity of hypostoichiometric low pu content (U, Pu) $\text{O}_{2-x}$  mixed oxide”, *J. Nucl. Mater.*, vol. 277, no. 2–3, pp. 143–158, 2000.
- [35] M. Inoue, “Thermal conductivity of uranium-plutonium oxide fuel for fast reactors”, *J. Nucl. Mater.*, vol. 282, no. 2–3, pp. 186–195, 2000.
- [36] C. Cozzo *et al.*, “Thermal diffusivity of homogeneous SBR MOX fuel with a burnup of 35 MWd/kgHM”, *J. Nucl. Mater.*, vol. 400, no. 3, pp. 213–217, 2010.
- [37] D. Staicu *et al.*, “Preparing ESNII for HORIZON 2020 - Deliverable D7.4.2 - Properties measurements on irradiated fuels (NESTOR 3)”, ESNII+ Deliverable, 2017.
- [38] T. Tachibana, T. Ohmori, S. Yamanouchi, and T. Itaki, “Determination of melting point of mixed-oxide fuel irradiated in fast breeder reactor”, *J. Nucl. Sci. Technol.*, vol. 22, no. 2, pp. 155–157, 1985.
- [39] K. Konno and T. Hirosawa, “Melting temperature of irradiated fast reactor mixed oxide fuels”, *J. Nucl. Sci. Technol.*, vol. 35, no. 7, pp. 494–501, 1998.

- [40] M. Kato, K. Morimoto, H. Sugata, K. Konashi, M. Kashimura, and T. Abe, “Solidus and liquidus of plutonium and uranium mixed oxide”, *J. Alloys Compd.*, vol. 452, no. 1, pp. 48–53, 2008.
- [41] M. Kato, K. Morimoto, H. Sugata, K. Konashi, M. Kashimura, and T. Abe, “Solidus and liquidus temperatures in the  $\text{UO}_2\text{-PuO}_2$  system”, *J. Nucl. Mater.*, vol. 373, no. 1–3, pp. 237–245, 2008.
- [42] T. Hirosawa and I. Sato, “Burnup dependence of melting temperature of FBR mixed oxide fuels irradiated to high burnup”, *J. Nucl. Mater.*, vol. 418, no. 1–3, pp. 207–214, 2011.
- [43] D. Prieur *et al.*, “Linear thermal expansion, thermal diffusivity and melting temperature of Am-MOX and Np-MOX”, *J. Alloys Compd.*, vol. 637, pp. 326–331, 2015.
- [44] Y. Philipponneau, “Thermal conductivity of  $(\text{U, Pu})\text{O}_{2-x}$  mixed oxide fuel”, *J. Nucl. Mater.*, vol. 188, pp. 194–197, Jun. 1992.
- [45] W. E. Ellis, J. D. Porter, and T. L. Shaw, “The effect of oxidation, burnup and poisoning on the thermal conductivity of  $\text{UO}_2$ : a comparison of data with theory”, in: *Proc. of LWRFP meeting, Park City, Utah, USA, 10-13 April 2000*, pp. 1–15, 2000.
- [46] A. R. Massih, “ $\text{UO}_2$  fuel oxidation and fission gas release”, Swedish Radiation Safety Authority report, Report number 2018:25, 2018.
- [47] A. Resnick, K. Mitchell, J. Park, E. B. Farfán, and T. Yee, “Thermal transport study in actinide oxides with point defects”, *Nucl. Eng. Technol.*, vol. 51, no. 5, pp. 1398–1405, 2019.
- [48] J.-M. Bonnerot, “Propriétés thermiques des oxydes mixtes d’uranium et de plutonium”, PhD thesis, 1988.
- [49] MathWorks, “MATLAB code”, 2019. [Online]. Available: <https://uk.mathworks.com/products/matlab.html>.
- [50] The R Foundation, “R version 3.5.1”, 2018. [Online]. Available: <https://www.r-project.org/>.
- [51] P. Pernot and F. Cailliez, “A critical review of statistical calibration/prediction models handling data inconsistency and model inadequacy”, *AIChE J.*, vol. 63, no. 10, pp. 4642–4665, 2017.
- [52] OECD/NEA, “NEA Halden Reactor Project”, 2019. [Online]. Available: <https://www.oecd-nea.org/jointproj/halden.html>.
- [53] OECD/NEA, “International Fuel Performance Experiments (IFPE) database”, 2017. [Online]. Available: <https://www.oecd-nea.org/science/wprs/fuel/ifpelst.html>.
- [54] E. Kolstad and C. Vitanza, “Fuel rod and core materials investigations related to LWR extended burnup operation”, *J. Nucl. Mater.*, vol. 188, pp. 104–112, 1992.
- [55] D. Baron, “About the modelling of fuel thermal conductivity degradation at high-burnup accounting for recovering process with temperature”, in: *Proc. Seminar on Thermal Performance of High Burnup LWR Fuel, OECD-NEA, Cadarache, France, 3-6 March 1998*, p. 129, 1998.
- [56] GIF (Generation IV International Forum), “Technology Roadmap Update for Generation IV Nuclear Energy Systems”, 2014.
- [57] Institut de Radioprotection et de Sureté Nucléaire, “Review of Generation IV Nuclear Energy Systems”, 2015.
- [58] J. Fink, “Thermophysical properties of uranium dioxide”, *J. Nucl. Mater.*, vol. 279, no. 1, pp. 1–18, 2000.
- [59] C. O. T. Galvin, P. A. Burr, M. W. D. Cooper, P. C. M. Fossati, and R. W. Grimes, “Using Molecular Dynamics to Predict the Solidus and Liquidus of Mixed Oxides  $(\text{Th,U})\text{O}_2$ ,  $(\text{Th,Pu})\text{O}_2$  and  $(\text{Pu,U})\text{O}_2$ ”, *J. Nucl. Mater.*, vol. 534, 152127, 2020.
- [60] D. Manara, C. Ronchi, M. Sheindlin, M. Lewis, and M. Brykin, “Melting of stoichiometric and hyperstoichiometric uranium dioxide”, *J. Nucl. Mater.*, vol. 342, no. 1–3, pp. 148–163, 2005.

- [61] C. T. Walker, “Assessment of the radial extent and completion of recrystallisation in high burnup  $\text{UO}_2$  nuclear fuel by EPMA”, *J. Nucl. Mater.*, vol. 275, no. 1, pp. 56–62, 1999.
- [62] J. Noirot, L. Desgranges, and J. Lamontagne, “Detailed characterization of high burnup structures in oxide fuels”, *J. Nucl. Mater.*, vol. 372, no. 2–3, pp. 318–339, 2008.
- [63] F. Lemoine, D. Baron, and P. Blanpain, “Key parameters for the High Burnup Structure formation thresholds”, in: *Proc. 2010 LWR Fuel Performance Meeting/Top Fuel/WRFPM, 26-29 September 2010, Orlando, Florida, USA, 2010*.
- [64] M. Tourasse, M. Boidron, and B. Pasquet, “Fission product behaviour in Phenix fuel pins at high burnup”, *J. Nucl. Mater.*, vol. 188, pp. 49–57, 1992.
- [65] D. C. Fee and C. E. Johnson, “Fuel-cladding chemical interaction in uranium-plutonium oxide fast reactor fuel pins”, *J. Nucl. Mater.*, vol. 96, no. 1–2, pp. 80–104, 1981.
- [66] T. Uwaba, M. Ito, and K. Maeda, “Diametral strain of fast reactor MOX fuel pins with austenitic stainless steel cladding irradiated to high burnup”, *J. Nucl. Mater.*, vol. 416, no. 3, pp. 350–357, 2011.
- [67] Y. Guerin, “Fuel Performance of Fast Spectrum Oxide Fuel”, in *Comprehensive Nuclear Materials*, 2012.
- [68] R. Parrish and A. Aitkaliyeva, “A review of microstructural features in fast reactor mixed oxide fuels”, *J. Nucl. Mater.*, vol. 510, pp. 644–660, 2018.
- [69] M. Teague, B. Gorman, J. King, D. Porter, and S. Hayes, “Microstructural characterization of high burnup mixed oxide fast reactor fuel”, *J. Nucl. Mater.*, vol. 441, no. 1–3, pp. 267–273, 2013.
- [70] M. Inoue, K. Maeda, K. Katsuyama, K. Tanaka, K. Mondo, and M. Hisada, “Fuel-to-cladding gap evolution and its impact on thermal performance of high burnup fast reactor type uranium – plutonium oxide fuel pins”, *J. Nucl. Mater.*, vol. 326, pp. 59–73, 2004.
- [71] K. Maeda, K. Tanaka, T. Asaga, and H. Furuya, “Distributions of volatile fission products in or near the fuel-cladding gap of the FBR MOX fuel pins irradiated to high burnup”, *J. Nucl. Mater.*, vol. 344, pp. 274–280, 2005.
- [72] J.-C. Dumas, “Etude des conditions de formation du Joint Oxyde-Gaine dans les combustibles des Reacteurs à Neutrons Rapides (Observations et propositions d’un modèle de comportement des produits de fission volatils)”, PhD thesis, 1992.
- [73] T. N. Pham Thi, “Caractérisation et modélisation du comportement thermodynamique du combustible RNR-Na sous irradiation”, PhD thesis, 2014.
- [74] C. Guéneau *et al.*, “Thermodynamic modelling of advanced oxide and carbide nuclear fuels: Description of the U-Pu-O-C systems”, *J. Nucl. Mater.*, vol. 419, no. 1–3, pp. 145–167, 2011.
- [75] A. L. Smith *et al.*, “Structural and thermodynamic study of dicesium molybdate  $\text{Cs}_2\text{Mo}_2\text{O}_7$ : Implications for fast neutron reactors”, *J. Solid State Chem.*, vol. 253, no. May, pp. 89–102, 2017.
- [76] T. Ishii and T. Mizuno, “Thermal conductivity of cesium molybdate  $\text{Cs}_2\text{MoO}_4$ ”, *J. Nucl. Mater.*, vol. 231, no. 3, pp. 242–244, 1996.
- [77] T. Ishii and T. Mizuno, “An investigation of the thermal conductivity of  $\text{Cs}_2\text{MoO}_4$ ”, *J. Nucl. Mater.*, vol. 247, pp. 82–85, 1997.
- [78] K. Maeda and T. Asaga, “Change of fuel-to-cladding gap width with the burnup in FBR MOX fuel irradiated to high burnup”, *J. Nucl. Mater.*, vol. 327, no. 1, pp. 1–10, 2004.
- [79] J. Lavarenne *et al.*, “A 2-D correlation to evaluate fuel-cladding gap thermal conductance in mixed oxide fuel elements for sodium-cooled fast reactors”, in *Proceedings of Global/Top Fuel 2019, 22-27 September 2019, Seattle, Washington, USA, 2019*.
- [80] A. Karahan, “Modeling of thermo-mechanical and irradiation behavior of metallic and oxide fuels for sodium fast reactors”, PhD thesis, 2009.

- [81] A. Karahan and J. Buongiorno, “Modeling of thermo-mechanical and irradiation behavior of mixed oxide fuel for sodium fast reactors”, *J. Nucl. Mater.*, vol. 396, no. 2–3, pp. 272–282, 2010.
- [82] G. Wallez, P. E. Raison, A. L. Smith, N. Clavier, and N. Dacheux, “High-temperature behavior of cesium molybdate  $\text{Cs}_2\text{MoO}_4$ : Implications for fast neutron reactors”, *J. Solid State Chem.*, vol. 215, pp. 225–230, 2014.
- [83] M. Lainet, B. Michel, J. C. Dumas, M. Pelletier, and I. Ramière, “GERMINAL, a fuel performance code of the PLEIADES platform to simulate the in-pile behaviour of mixed oxide fuel pins for sodium-cooled fast reactors”, *J. Nucl. Mater.*, vol. 516, pp. 30–53, 2019.
- [84] T. Uwaba, J. Nemoto, I. Ishitani, and M. Ito, “Coupled computer code study on irradiation performance of a fast reactor mixed oxide fuel element with an emphasis on the fission product cesium behavior”, *Nucl. Eng. Des.*, vol. 331, no. February, pp. 186–193, 2018.
- [85] D. Pizzocri, T. Barani, and L. Luzzi, “SCIANTIX code”, 2018. [Online]. Available: <https://gitlab.com/poliminrg/sciantix>.
- [86] T. R. Pavlov, F. Kremer, R. Dubourg, A. Schubert, and P. Van Uffelen, “Towards a More Detailed Mesoscale Fission Product Analysis in Fuel Performance Codes: a Coupling of the TRANSURANUS and MFPR-F Codes”, in *TopFuel2018 - Reactor Fuel Performance*, pp. 1–9, 2018.